Aus der Radiologischen Klinik
(Geschäftsführender Direktor: Prof. Dr. med. Dr. rer. nat. Jürgen Debus)
Abteilung für Radioonkologie und Strahlentherapie
(Ärztlicher Direktor: Prof. Dr. med. Dr. rer. nat. Jürgen Debus)

Daily adaptive magnetic resonance-guided radiotherapy – analysis of patient benefit

Inauguraldissertation
zur Erlangung des Doctor scientiarum humanarum (Dr. sc. hum.)
an der
Medizinischen Fakultät Heidelberg
der
Ruprecht-Karls-Universität

vorgelegt von
Carolin Julia Buchele

aus
Göppingen

2024

Dekan: Prof. Dr. rer. nat. Michael Boutros

Doktorvater: Prof. Dr. rer. nat. Markus Alber

CONTENTS

ABBREVIATIONS

2D	2-dimensional
3D	3-dimensional
BED	Biological effective dose
CBCT	Cone beam computed tomography
CT	Computed tomography
CTV	Clinical tumor volume
DICOM	Digital imaging and communications in medicine
GTV	Gross tumor volume
IGRT	Image guided radiotherapy
IMRT	Intensity modulated radiotherapy
IQR	Interquartile range
ITV	Internal target volume
kV	Kilovoltage
Linac	Linear accelerator
MLC	Multi leaf collimator
MR	Magnetic resonance
MRgRT	Magnetic resonance-guided radiotherapy
MRI	Magnetic resonance image
MV	Megavoltage
OAR	Organ at risk
PRV	Planning organ at risk volume
PTV	Planning target volume
ROI	Region of interest
RoM	Range of movement
SBRT	Stereotactic body radiotherapy
TPS	Treatment planning system
TRUFI	True fast imaging with steady state precession

1 INTRODUCTION

1.1 Image guided radiotherapy and stereotactic body radiotherapy

Image guided radiotherapy (IGRT) is the current gold standard in radiotherapy. Imaging plays an important role throughout the entire treatment process of a patient, from the diagnosis of the lesions to be treated, through generation of treatment plans to imaging in the treatment room before or during treatment delivery. One of the major foundations of this development was the introduction of computed tomography (CT) in 1972 (Hounsfield 1973). In contrast to conventional methods at the time such as 2-dimensional (2D) simulator films, it provided an accurate visualization of internal anatomical structures and therefore a more exact localization of tumors and surrounding organs (Dobbs et al. 1983; Rockoff 1977). In addition, CT images offered information on the electron density of tissues and as a result enabled the calculation of dose distributions that were based on the patient-specific geometries and were able to take into account tissue inhomogeneities (Battista et al. 1980; Jelden et al. 1976). This also constituted the first steps towards 3-dimensional (3D) dose calculation and was one of the requirements for more complex planning techniques like intensity modulated radiation therapy (IMRT), which applies inverse optimization algorithms to generate the treatment plan (Dawson and Menard 2010).

Another step towards the current standards in IGRT was the development of cone beam computed tomography (CBCT), which combined a kilovoltage (kV) X-ray tube and a flat panel detector, both mounted on the linear accelerator for in-room volumetric imaging (Jaffray et al. 1999). Compared to other on-line imaging modalities, which had previously been used, like megavoltage (MV) portal imaging, CBCT provided a better soft tissue contrast, allowing more accurate positioning of the patient for treatment delivery. It further enabled the detection of interfractional changes like weight loss, changes in tumor volume or in position of surrounding organs at risk (Dawson and Menard 2010). As a consequence, the impact of these changes could be assessed regularly and a possible need to adjust the treatment plan could be recognized. Current in-room imaging possibilities include MV CT imaging, orthogonal kV imaging and more recently magnetic resonance (MR) imaging in addition to CBCT imaging.

Image guided radiotherapy also played an important role in the transfer of intracranial stereotactic radiosurgery treatments to extracranial locations. Various definitions of stereotactic body radiotherapy (SBRT) can be found in previous reports, but all share some common features. They define SBRT as a radiotherapy treatment of extracranial target volumes with high doses in only a few fractions (Benedict et al. 2010; Guckenberger et al. 2020; Kirkbride and Cooper 2011). Furthermore, high precision is required throughout the whole treatment process for example by applying state-of-the-art imaging techniques.

The concept of stereotactic radiosurgery was first introduced by Lars Leksell in the 1950s (Leksell 1951; Solberg et al. 2012). A stereotactic frame fixed to the patient's skull was applied for exact localization of the treated lesions, which was adapted from neurosurgical treatments. This method was adjusted for extracranial tumor locations like liver or lung in the 1990s (Blomgren et al. 1995; Lax et al. 1994). A stereotactic body frame combined with abdominal compression was applied to achieve localization of the tumor with similar precision compared to intracranial stereotactic treatments. The introduction of CBCT for in-room imaging additionally increased precision of target localization in extracranial stereotactic body radiotherapy (SBRT) and therefore the possibility to reduce safety margins for future SBRT treatments was discussed (Guckenberger et al. 2006; Guckenberger et al. 2008).

By now SBRT has become an important element in the treatment of various extracranial lesions such as lung and liver tumors, pancreatic and prostate cancer. For instance, SBRT is an effective treatment for liver metastases with high local control rates being reported (Katz et al. 2007; Rusthoven et al. 2009). Similarly, SBRT can achieve high local control rates in the treatment of pulmonary lesions (Guckenberger et al. 2009; Hof et al. 2003) and has become a standard treatment for inoperable early stage lung cancer (Daly 2022; Pollard et al. 2017; Regnery et al. 2022b). Additionally, many lesions show a clear dose-response relationship and require a high biological effective dose (BED) to achieve high local control rates. For pulmonary lesions, a higher local control and overall survival can be achieved by applying a BED greater than 100 Gy compared to lower dose prescriptions. In treatments of liver metastases, a BED greater than 100 Gy also leads to significantly improved local control and overall survival rates (Kok et al. 2020; Ohri et al. 2021; Su et al. 2021). Similarly, for the treatment of adrenal metastases a BED over 100 Gy is recommended to achieve high local control rates (Chen et al. 2020; Stumpf et al. 2021).

However, the dose that can be applied to the tumor is often limited due to surrounding organs at risk (OAR). SBRT treatments of pulmonary lesions which are close to the proximal bronchial tree are associated with a high risk of severe toxicity in the central airways or the esophagus (Haseltine et al. 2016; Lindberg et al. 2021; Timmerman et al. 2006). In some cases, these toxicities might even cause the death of the patient. In SBRT treatments of abdominal lesions either coverage of the planning target volume (PTV) or even the total prescribed dose needs to be reduced if gastrointestinal organs like stomach, small bowel or duodenum are situated in close proximity to the tumor (Miften et al. 2021). Radiation induced toxicities of these organs include nausea, vomiting, mucositis, ulceration or perforation (Kavanagh et al. 2010; Lo et al. 2013; Michel et al. 2017; Thomas et al. 2014). The occurrence of adverse effects could be favored by uncertainties in the treatment process. In particular, interfractional changes in patient geometry like deformations of the target volume, differences in OAR positions relative to the treated lesion or differences in breathing phase prove to be a challenge in SBRT treatments.

1.2 Magnetic resonance-guided radiotherapy

The introduction of linear accelerators with integrated MR imaging (MR-linac) offers the possibility to reduce some uncertainties in the treatment process. MR imaging provides a better soft tissue contrast compared to conventional X-ray based systems for in-room imaging and no additional dose needs to be applied. This allows for precise delineation of target volumes and OARs based on MR images acquired before treatment. As a result, treatment plans can be adapted daily to the current patient geometry with the patient remaining on the treatment couch during adaptation. Previous studies found that plan adaptation led to significantly improved target volume coverage, while simultaneously reducing the dose to organs at risk. For adrenal metastases, Palacios et al. found that target volume coverage could be improved in around two thirds of adapted fractions (Palacios et al. 2018). At the same time, the dose to OARs could be significantly reduced to meet institutional constraints. Similar results were reported by Henke et al. in treatments of liver and other abdominal metastases (Henke et al. 2018a). Violations of OAR dose constraints when calculating the base plan on the daily patient anatomy, were identified as the main reason for adaptation in this study. Other research on magnetic resonance-guided radiotherapy (MRgRT) treatments lesions situated in various locations in the thorax and abdomen also confirmed the need for adaptation in a large majority of fractions (Hoegen et al. 2023; Mayinger et al. 2021; Nierer et al. 2022; Padgett et al. 2020; Regnery et al. 2022a;

Regnery et al. 2021; Weykamp et al. 2022). The main causes for adaptation also included improved target volume coverage and failure to meet OAR dose constraints.

In addition, MR-linacs provide the possibility of continuous imaging during irradiation, which enables respiratory gated treatment delivery. When treating the patient without respiratory gating, tumor movement needs to be accounted for by defining an internal target volume (ITV), which includes differences in tumor positions and shape due to breathing (Landberg et al. 1999). However, the irradiated volume is relatively large when an ITV is used and it possibly overlaps with organs at risk. Therefore, either target volume coverage would have to be reduced or higher doses to OARs would have to be accepted compared to respiratory gated treatments (Spindeldreier et al. 2021). Furthermore, Cusumano et al. found that some movements induced by breathing e.g. baseline drifts might not be sufficiently compensated by the application of an ITV and respiratory gating could be more beneficial in treatments of these lesions (Cusumano et al. 2018).

Overall, the combination of daily plan adaptation and motion management allows for a reduction of large PTV margins that were necessary to account for inter- and intrafractional uncertainties (Acharya et al. 2016; Corradini et al. 2019; Kashani and Olsen 2018). This could also reduce the dose to surrounding OARs and thereby the risk of complications as described in the previous chapter.

1.2.1 Technical aspects of the 0.35 T MR-linac

Although the concept of a hybrid device, combining a linear accelerator with MR imaging, was first discussed in 2000 (Lagendijk and Bakker 2000), implementation in clinical practice took until 2017, when first patients were treated with an MR-linac (PR Newswire 2017). Initially, two MR-linacs from different manufacturers were commercially available. The Elekta Unity combines a 1.5 T MR scanner with a 7 MV linac, while the ViewRay MRIdian (ViewRay, Inc., Cleveland, OH) integrates a 0.35 T MR scanner with a 6 MV linac. Both systems use different strategies to solve technical challenges arising from the integration of MR imaging with a linear accelerator. Since this research was performed on the ViewRay MRIdian, this system is described in more detail.

One of the technical challenges that had to be solved is the shielding of linac components such as the magnetron, from the magnetic field because proper functioning would be impaired otherwise (Klüter 2019). At the same time, RF noise generated by these linac components could cause problems with MR image quality. Therefore, shielding in the other direction is also required. The 0.35 T MR-linac manufactured by ViewRay solved these issues by arranging the linac components in six so-called buckets located on a ring gantry. These cylindric buckets are made of ferromagnetic material and have additional layers of carbon fiber and copper, which are used for RF shielding. The ring gantry is situated between the two halves of a split magnet (Figure 1). Both halves are thermally and mechanically connected to ensure stability of the magnetic field (Wen et al. 2018).

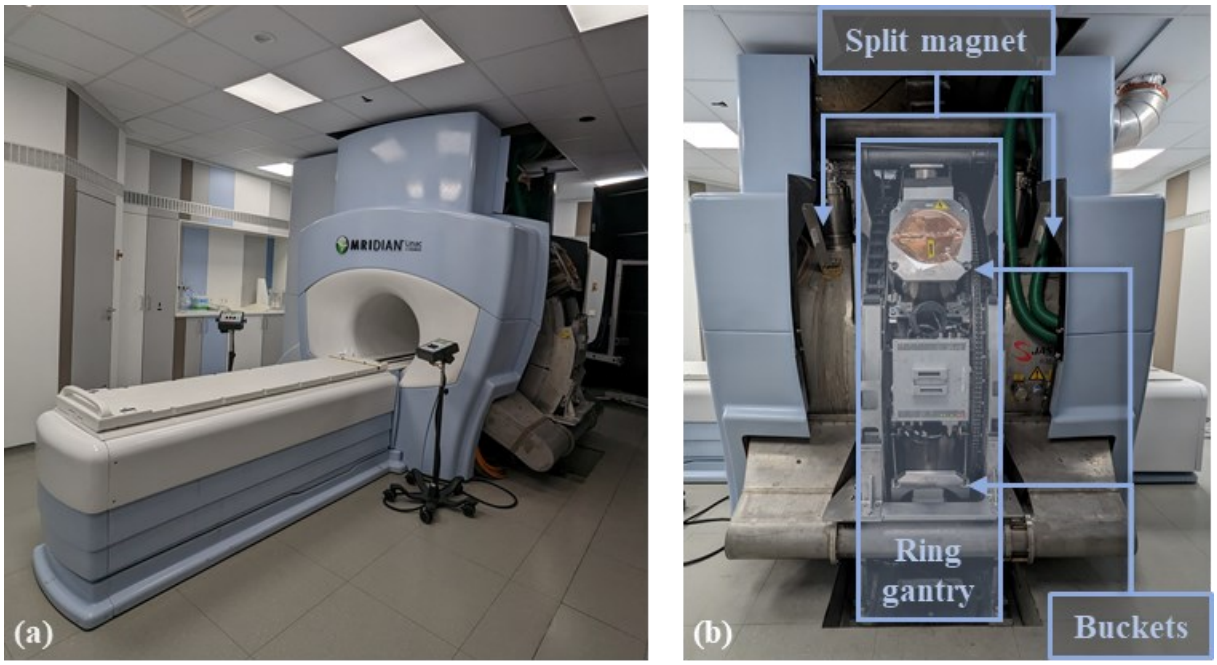

Figure 1: (a) Image of 0.35 T MR-linac (ViewRay MRIdian) installed at Heidelberg University Hospital with opened cover on the right side. (b) View below the cover of the MR-linac. Ring gantry with buckets sitting between the halves of the split magnet.

The bore has a diameter of 70 cm and a Field of View with a diameter of 50 cm (Klüter 2019). A True Fast Imaging with Steady State Precession (TRUFI) sequence with a T_2/T_1 weighted contrast is used for acquisition of 3D MR images as well as for 2D cine images acquired during irradiation. For volumetric MR images various image resolutions are available with in-plane voxel length and slice thicknesses between 1.5 and 3.0 mm. At Heidelberg University Hospital the sequences that are used most commonly have a resolution of 1.5 x 1.5 x 3.0 mm^3 with an acquisition time around 25 seconds for images that are acquired with the patients holding their

breath. A resolution of 1.5 x 1.5 x 1.5 mm^3 with acquisition times around three minutes is routinely used for images which are acquired with the patient breathing freely. Two-dimensional cine MR images can be acquired during irradiation in up to three different planes with two to eight frames per second depending on the number of planes used for imaging. These cine images are used for automatic beam gating during treatment delivery.

The linear accelerator delivers a photon beam with and energy of 6 MV and a dose rate of around 600 cGy/min (Klüter 2019). No flattening filter is used to flatten the beam profile. A double-stack, double-focused multi leaf collimator (MLC) with 138 tungsten alloy leaves is used to shape the treatment beam. The MLC allows field sizes of up to 27.4 x 24.1 cm^2, while the minimum field size is 0.2 x 0.415 cm^2.

The treatment beam is oriented perpendicular to the magnetic field (Klüter 2019). While uncharged photons are not affected by this assembly, the magnetic field does have an effect on secondary electrons generated inside the patient. Trajectories of these electrons are changed due to the Lorentz force which affects charged particles in a magnetic field. In homogeneous materials, a perpendicular magnetic field can lead to changes in the dose distribution like a reduced build-up distance as well as a small shift and increase of the penumbra (Raaymakers et al. 2004). In inhomogeneous materials with water-air or tissue-air boundaries, a dose increase can be observed at the surface boundaries (Raaijmakers et al. 2005). The trajectory of electrons is changed due to the Lorentz force and they are forced towards the tissue surface. This effect is called Electron Return Effect and it is dependent on magnetic field strength (Raaijmakers et al. 2008). Although the effect is less pronounced in a field strength of 0.35 T, it still has to be accounted for during plan optimization. The ViewRay treatment planning system (TPS) uses a fast Monte Carlo based dose calculation algorithm for this purpose (Klüter 2019). The KMC Monte Carlo implementation uses variance reduction techniques to reduce calculation times and thus enable IMRT dose calculation in a few minutes (Kawrakow 2001; Kawrakow and Fippel 2000; Wang et al. 2016).

1.2.2 Treatment Simulation and Planning

Treatment simulation is usually performed one week prior to the first treatment on the MR-linac. A 3D MR image is acquired in inspiration breath hold for moving lesions in the thorax or upper abdomen to reduce motion artefacts. Imaging of lesions with no or only limited mobility can be performed with the patient breathing freely. At least two MR images are acquired for each patient. In some cases, imaging is repeated multiple times to verify that the patient can tolerate remaining in the treatment position for a longer period of time. Additionally, a 2D cine is performed to check if the patient can reach the same breath-hold position repeatedly and if the treated lesion is suitable for respiratory beam gating. If the lesion is not visible on cine images, a surrogate structure with correlating movement pattern is selected. A CT image is acquired afterwards and deformably registered to the MR image, in order to provide the electron density information necessary for dose calculation.

Organs at risk as well as the gross tumor volume (GTV) are contoured on one of the MR images acquired during simulation. The clinical tumor volume (CTV) contour is created by adding margin between two and five millimeters to the GTV, depending on the type of lesion treated. The CTV is subsequently expanded by three millimeters, creating the PTV contour. OAR tolerance doses as well as dose prescription to the PTV are determined by the physician. For inhomogeneous treatments, at least 95% of the PTV should receive the prescribed dose, while usually allowing inhomogeneities of up to 125%. Inhomogeneities of up to 154% of the prescribed dose are allowed for certain lesions that are located far away from any organs at risk. However, if organs at risk are close to or overlapping with the PTV, the coverage might need to be reduced below 95% in order to meet OAR dose constraints.

An inverse optimization algorithm is used to create a step and shoot IMRT plan. Typically, multiple iterations are necessary until OAR dose constraints are met and PTV coverage and dose distribution of the plan are acceptable. The finalized plan is approved by the physician and a patient-specific quality assurance measurement is performed.

1.2.3 Adaptive Workflow

Each adaptive treatment starts with the acquisition of a 3D MR image with the same sequence parameters that have been employed for treatment planning images. The GTV is then used as a reference structure to register the daily MR image (MRI_A) to the image of the base plan. Subsequently, OARs are deformably transferred to MRI_A, while GTV, CTV and PTV are transferred rigidly. OAR and target volume contours are reviewed and adjusted to the current anatomy. This step can be quite time consuming depending on the number and complexity of OARs to be recontoured. Therefore, recontouring of OARs is only performed in a certain area, termed PTV_{Expand}, which encompasses the PTV expanded by 3 cm in lateral and anterior-posterior direction and 1cm in cranio-caudal direction (Bohoudi et al. 2017).

The base plan is then calculated on the daily MR image. If either OAR tolerance dose is violated or the PTV is insufficiently covered by the prescription isodose, the base plan is reoptimized until dose constraints are met. In those cases that already had a reduced PTV coverage in the base plan due to surrounding OARs, the aim of reoptimization is to achieve a dose coverage value that is comparable to the base plan. After the reoptimized plan is approved by the physician, a secondary dose calculation is performed as quality assurance. Until the beginning of 2023, an in house developed tool was used to additionally check certain plan parameters, which are not detected through secondary dose calculation, like the occurrence of gaps in OAR contours or number of small beam segments (Rippke et al. 2022). However, it is not possible to use this tool anymore due to an update of the treatment software, which does not allow export of any treatment information before the treatment session is finished. Therefore, a more time-consuming visual inspection of the plan needs to be performed.

A second pre-irradiation image is acquired (MRI_{pl}) to verify patient position and make small adjustments if necessary. Since this step is not included in the adaptive workflow designed by the manufacturer, the adapted plan needs to be closed and reloaded again on the treatment console. Therefore, MR images for position verification immediately before irradiation are not necessarily acquired regularly at other sites. At rare intervals, treatment needs to be interrupted at this point and the adaptive workflow started from the beginning due to large displacements or deformations of OARs (Figure 2).

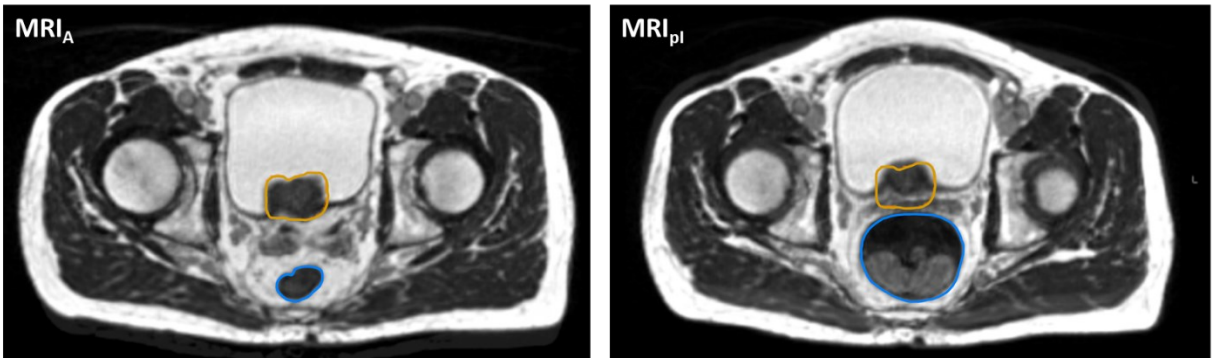

Figure 2: Axial slices of MRI_A and MRI_{pI} acquired during the same treatment fraction. The rectum (blue) is significantly closer to the CTV (orange) due to large changes in OAR volume from MRI_A to MRI_{pI}. Patient treatment was therefore interrupted after acquisition of MRI_{pI}.

Smaller changes in OAR position are usually accepted after visual inspection and do not lead to interruption of treatment. Subsequently, irradiation is started. Real-time structure tracking and beam gating are available during treatment delivery. The tracking structure is expanded by a certain margin to create the gating boundary. Only a certain percentage of the tracking structure is allowed outside the boundary until the beam turns off. Usually, the GTV is used as a tracking structure, a margin of 3 mm is applied and allowed percentage outside the boundary is 3%. An overview of the previously described workflow can be found in Figure 3.

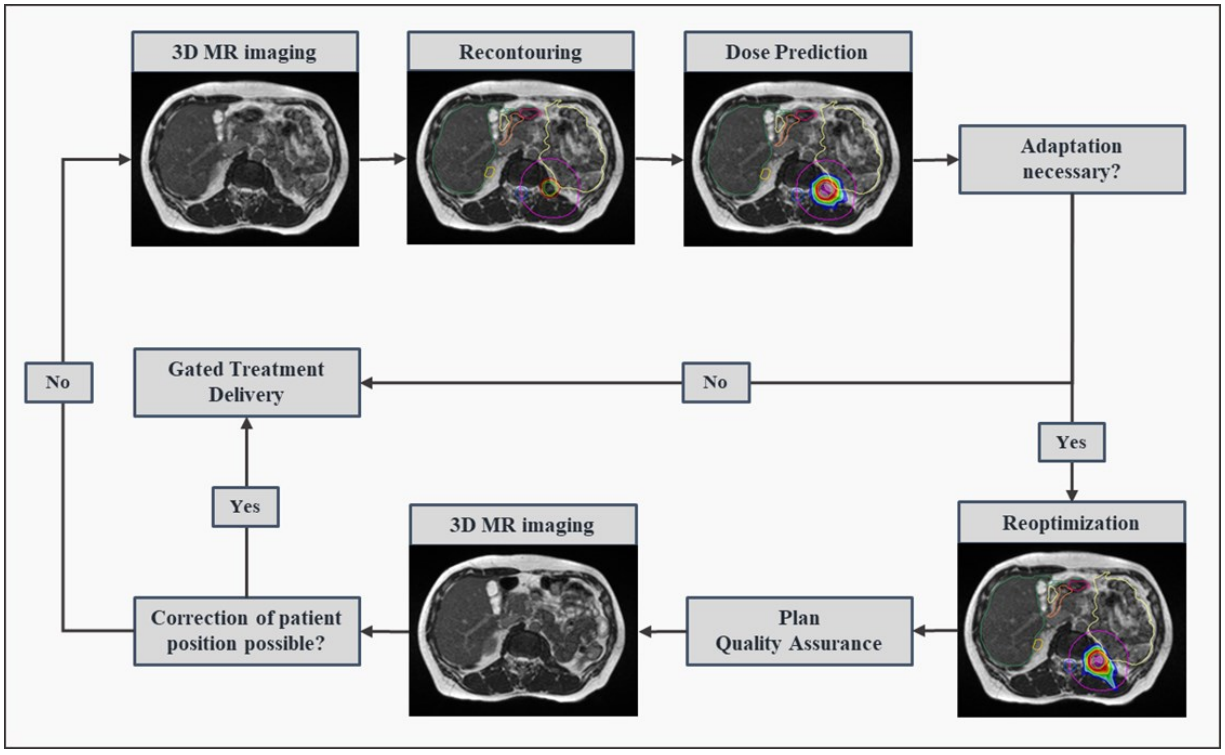

Figure 3: Overview of the adaptation workflow from acquisition of the first MR image to treatment delivery.

1.3 Aim

The ability to compensate for interfractional changes is one major advantage of adaptive MR-guided radiotherapy. The treatment plan can be adjusted to positional variations and deformations of target volumes and organs at risk for each fraction. However, patient geometry may also change during the adaptation process. In particular, gastrointestinal organs such as stomach, small bowel and duodenum might exhibit major positional shifts (Alam et al. 2022; Uchinami et al. 2023). Median displacements of up to 14 mm within a maximum time span of 16.5 minutes were determined for these organs by Uchinami et al. (Uchinami et al. 2023). Although intrafractional organ movements of this magnitude could possibly lead to distinctly higher organ doses for OARs in close proximity to treated lesions, there is only a limited number of studies investigating the dosimetric impact of organ movement occurring during the adaptation process. For treatments of pancreatic cancer, violations of OAR dose constraints due to intrafractional changes were found in one-third to one half of evaluated fractions (Teoh et al. 2022; Tyagi et al. 2021). In certain cases, the occurrence of intrafractional organ movement and resulting constraint violations could reduce or even negate the benefit gained from adaptation. Therefore, the following hypothesis will be tested in this study:

“For some cases adaptation has no benefit”

Since fewer fractions are delivered in SBRT treatments compared to normo-fractionated treatment schedules, OAR constraint violations in single fractions possibly have a greater impact and therefore become more relevant. Furthermore, previously performed studies suggest that tolerance doses are regularly not met due to intrafractional organ movement. As a consequence, these movements might have to be compensated by using a planning organ at risk volume (PRV), which includes possible locations the OAR might occupy during treatment (Landberg et al. 1999). In order to assess the impact of intrafractional changes and generate patient-specific PRVs to achieve more robust adaptation results, the extent of organ movement needs to be determined before the first adaptive treatment. MR images acquired during simulation might provide the opportunity to do so. No additional dose is delivered to the patient compared to X-ray based imaging methods and a larger number of images can be acquired to evaluate positional changes of OARs. As major shifts in organ position can occur within a short time frame (Mostafaei et al. 2018; Uchinami et al. 2023), it might be possible to determine at least the range of organ movement during adaptive treatments in advance using multiple

simulation MR images, although simulation sessions are considerably shorter. This leads to the second hypothesis to be investigated:

“More robust adaptive treatments can be obtained by predicting the extent of intrafractional organ movement before the first treatment”

However, the question arises whether compensation of intrafractional organ movement is necessary at all, or whether it could be more effective to reduce the time of adaptive treatments. Currently, the adaptation process in MRgRT takes quite long with reported adaptation times of one hour or more (Henke et al. 2018a; Michalet et al. 2022a; Regnery et al. 2022a; Regnery et al. 2021; Tyagi et al. 2021). One of the main reasons for these long adaptation times is the lack of automation, which could significantly shorten various processes during adaptation. In particular, manual recontouring of OARs and target volumes takes a lot of time during adaptation. Therefore, it is often discussed whether the prolonged adaptation times might have a negative impact on the adaptation result due to the effect of intrafractional changes (Benitez et al. 2024; Chin et al. 2020; Guckenberger et al. 2024; Sritharan and Tree 2022). As major shifts in organ position, which could affect the adaptation result, can occur within a time frame that is significantly shorter than current adaptation times, this might not actually be the case. This results in the third hypothesis to be tested:

“Shorter adaptation times do not necessarily lead to more robust results”

The following investigation focuses specifically on the adaptive treatment of abdominal lesions, as surrounding gastrointestinal organs exhibit large displacements and deformations. Therefore, in these treatments a larger impact of intrafractional changes was expected compared to other tumor locations.

2 MATERIALS AND METHODS

2.1 Impact of plan adaptation and intrafractional changes on dose to organs at risk

Parts of chapters 2.1.1 and 2.1.3 were included in a publication (Buchele et al. 2024), which has been submitted to Radiation Oncology and is currently under review. Since the focus of this publication was on intrafractional changes, only two of the three dose distribution variants described in this chapter (adapt and pre-irradiation) were included. The remaining methodology including patient selection, creation of dose distribution variants, dose parameters and statistical analysis described in these chapters is identical to the methodology described in the publication.

2.1.1 Dose distribution variants

The effect of adaptation on OAR dose and the impact of intrafractional changes were evaluated using three variants of dose distribution – predicted, adapted and pre-irradiation dose distribution. The adapted dose distribution was extracted from the plan that was created during adaptation by optimizing the base plan to the anatomy of the day. The predicted and pre-irradiation dose distributions were not saved by the system automatically and therefore needed to be generated retrospectively. The predicted dose distribution was generated by calculating the base plan on the first MR image acquired during adaptation (MRI_A). Similarly, the pre-irradiation dose distribution was created by propagating the adapted plan on the second MR image acquired immediately before irradiation (MRI_{pI}). A schematic of the dose distribution variants and the plans and images used to create each variant can be found in Figure 4.

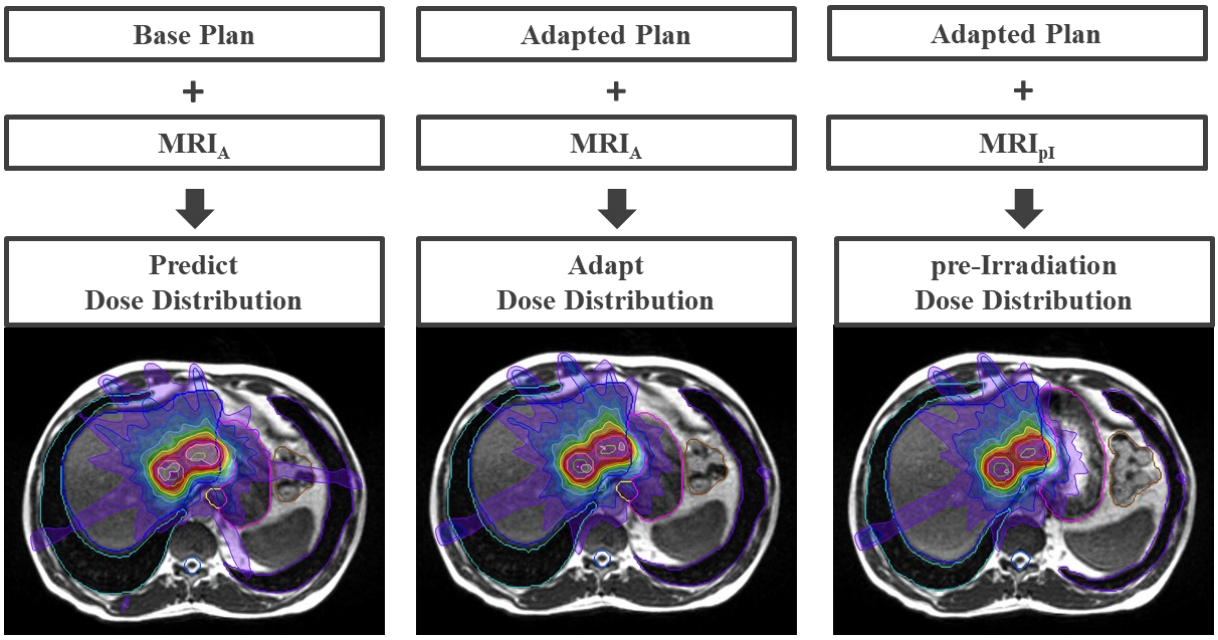

Figure 4: Overview over the three dose distribution variants created for analysis of changes in OAR dose and the respective plan and MR image used to generate each variant.

OAR dose parameters were extracted from each of the three dose distribution variants. A self-written script in MATLAB R2021a (The MathWorks, Inc., Natick, MA, USA) was used for this purpose since the dose parameters that were supposed to be evaluated could not be read out directly from the ViewRay TPS. Files in digital imaging and communications in medicine (DICOM) format which were previously exported from the TPS were used to reconstruct target volumes and OAR structures as well as the dose on the corresponding MR. Based on this reconstruction, dose parameters and minimal distances between OARs and GTV were calculated. One dose parameter which was determined for serial organs was the near-point maximum dose. This parameter was defined as the dose to a volume of 0.5 cm³ ($D_{0.5cc}$) for all serial OARs except the spinal cord, where near-point maximum dose was characterized as dose to a volume of 0.1 cm³ ($D_{0.1cc}$). In case of parallel organs, the mean OAR dose (D_{mean}) was determined.

In order to account for different fractionation schemes, all dose parameters, including dose differences, were assessed relative to the OAR tolerance dose of the respective dose fractionation. To differentiate between dose parameters of the three dose distribution variants, an index is used for each variant from this point on – “P” for predicted, “A” for adapted and “pI” for pre-irradiation dose distribution.

2.1.2 Explorative analysis of a limited number of patients with abdominal lesions

Five patients treated for liver metastases between February and June 2020 with online adaptive MR-guided RT were included in this analysis. A total of 26 adapted fractions were available for analysis, which concluded in 97 observations for each dose distribution. Lesions in close proximity to OARs as well as more lateral lesions farther away from OARs were selected. A dose of 50 Gy in five fractions was prescribed to the PTV for two patients. One patient received the same total dose in 10 fractions, allowing inhomogeneities up to 125% in all fractions. The other two patients received 45 Gy in three fractions with inhomogeneities up to 154%. A summary of fractionation schemes as well as respective OAR tolerance doses can be found in Table 1.

OARs were recontoured in all axial slices containing the PTV_{Expand} on MRI_A and MRI_{pI}. Organ contours outside these slices were deleted, except for the kidneys. As the mean dose was analyzed in this case, the complete OAR contour was maintained. For patient 2, the kidneys were excluded from analysis because they were located completely outside the axial slices defined by PTV_{Expand}.

The correlation between OAR dose relative to the tolerance dose and the distance between OAR and PTV was evaluated for each dose distribution variant. Additionally, the dose differences between adapted and predicted as well as between pre-irradiation and adapted variant were calculated and assessed in respect to the distance between OAR and PTV.

Table 1 Summary of treatment characteristics of the preliminary analysis.

Patient No.	Dose Prescription	OAR	Evaluated Dose Parameter	Tolerance Dose
1	5 x 10 Gy	Spinal Cord	$D_{0.1cc}$	27.0
		Stomach	$D_{0.5cc}$	35.0
		Small Bowel	$D_{0.5cc}$	35.0
		Duodenum	$D_{0.5cc}$	35.0
		Kidneys	D_{mean}	10.0
2	5 x 10 Gy	Spinal Cord	$D_{0.1cc}$	27.0
		Esophagus	$D_{0.5cc}$	34.0
		Heart	$D_{0.5cc}$	29.0
		Stomach	$D_{0.5cc}$	35.0
		Small Bowel	$D_{0.5cc}$	35.0
		Duodenum	$D_{0.5cc}$	35.0
3	10 x 5 Gy	Spinal Cord	$D_{0.1cc}$	35.0
		Stomach	$D_{0.5cc}$	42.5
		Small Bowel	$D_{0.5cc}$	43.5
		Duodenum	$D_{0.5cc}$	43.5
		Kidneys	D_{mean}	12.0
4	3 x 15 Gy	Spinal Cord	$D_{0.1cc}$	21.6
		Stomach	$D_{0.5cc}$	22.2
		Small Bowel	$D_{0.5cc}$	25.2
		Duodenum	$D_{0.5cc}$	22.2
		Kidneys	D_{mean}	8.5
5	3 x 15 Gy	Spinal Cord	$D_{0.1cc}$	21.6
		Stomach	$D_{0.5cc}$	22.2
		Small Bowel	$D_{0.5cc}$	25.2
		Duodenum	$D_{0.5cc}$	22.2
		Kidneys	D_{mean}	8.5

Overview over fractionation schemes, evaluated OARs and respective dose parameters as well as OAR tolerance doses for each patient.

2.1.3 Analysis of patients with abdominal lesions directly next to organs at risk

The focus of this analysis was on patients with various abdominal lesions, where at least one OAR was in close proximity to the treated lesion. Close proximity was defined as the OAR overlapping with the PTV in the base plan or at least one treatment fraction. This patient selection was based on the results of the previous evaluation with five patients, which can be found in chapter 3.1.1. In total, twenty patients with 151 adapted fractions were analyzed, including two patients from the previous analysis. The selected patients received online adaptive MRgRT between February 2020 and June 2021. Treated lesions were located in the liver, adrenal gland, abdominal lymph nodes or the pancreas. Evaluated OARs included small bowel, stomach, duodenum and esophagus. Since for some patients multiple OARs were in close proximity to the PTV, a total of 189 observations were evaluated. An overview over tumor localization, fractionation schemes, OARs and respective tolerance dose for each patient is shown in Table 2.

Identical to the adaptation workflow, recontouring of organs at risk was performed in the PTV_{Expand} area because only near-point maximum dose was examined and all OARs which were included in the analysis were close to the PTV. On MRI_A contours only had to be reviewed and adjusted, if necessary, since they were already segmented during adaptation. In contrast, contours needed to be newly segmented on MRI_{pI}.

For each dose distribution variant, the number of tolerance dose violations was determined in addition to the near-point maximum dose for the relevant OARs. McNemar mid-P test was performed in R (version 4.2.2.) using the ‘contingencytables’ package (Fagerland 2023) to evaluate if the occurrence of tolerance dose violations changed significantly between dose distribution variants (Fagerland et al. 2013).

Furthermore, the time difference between acquisition of MRI_A and MRI_{pI} was calculated because this duration corresponded with the time necessary to adapt the treatment plan. A linear mixed regression analysis was used to explore the effect of adaptation time on the difference between adapted and pre-irradiation dose. The model was fit in R using the ‘lme4’ package (Bates et al. 2015) with adaptation time as a fixed effect. OAR nested within patient was included as a random intercept to account for repeated measurements:

Dose Difference ~ Duration + (1 | Patient / OAR)

No obvious deviations from homoscedasticity or normality were detected in visual inspection of residual plots.

Additionally, a linear mixed effects analysis was performed to evaluate the relationship between dose distribution variant and OAR dose. The dose distribution variant was entered as a fixed effect. As in the previous model, OAR nested within patient was included as a random intercept:

Dose ~ Dose Distribution Variant + (1 | Patient / OAR)

This analysis was performed three times, once with predicted and adapted dose distribution variant, once for adapted and pre-irradiation variant and again for predicted and pre-irradiation variant. As with the previous model no deviations from homoscedasticity or normality were detected.

In addition, for each fraction the reason for changes to dose was determined. Those causes included OAR movement due to peristalsis, movement caused by large changes of stomach filling and incorrect matching from MRI_{pI} to MRI_{A} characterized by the OAR contour on MRI_{pI} overlapping with the GTV.

Table 2: Summary of treatment characteristics for patients with abdominal lesions.

Patient No.	Total dose (Gy)	No. of fractions	OAR	OAR tolerance dose (Gy)	Tumor localization
1	50	5	Stomach	35.0	Liver
			Duodenum	35.0	
			Esophagus	34.0	
2	50	5	Small bowel	35.0	Adrenal gland
3	50	5	Small bowel	35.0	Liver
4	50	5	Duodenum	35.0	Liver
5	50	5	Stomach	35.0	Liver
6	50	5	Stomach	35.0	Adrenal gland
7	50	5	Duodenum	35.0	Adrenal gland
8	50	5	Small bowel	35.0	Pancreas
9	50	10	Small bowel	43.5	Liver
10	50	10	Small bowel	43.5	Liver
11	50	10	Small bowel	43.5	Liver
12	50	10	Duodenum	43.5	Liver
13	50	10	Small bowel	43.5	Liver
			Duodenum	43.5	
14	50	10	Small bowel	43.5	Liver
15	50	10	Duodenum	43.5	Liver
16	50	10	Small bowel	43.5	Adrenal gland
			Stomach	42.5	
17	50	10	Small bowel	43.0	Liver
18	40	8	Stomach	40.0	Adrenal gland
			Small bowel	40.0	
19	35	7	Small bowel	37.0	Lymph Node Paracaval
20	30	6	Stomach	37.0	Lymph Node Porta hepatis

Overview over fractionation schemes, OARs, respective tolerance doses and tumor localization for each patient. Adapted from (Buchele et al. 2024)

2.2 Predictability of organ at risk movement during adaptation

The methods used to determine organ at risk movement which are described in this chapter were also a part of the aforementioned publication (Buchele et al. 2024). Main focus of this part of the publication was the comparison between range of movement during simulation and adaptation as well as correlation between simulation duration and range of organ movement during simulation sessions. The following chapter was expanded to also evaluate different methods to determine range of movement during simulation sessions and analyze the correlation between intrafractional dose changes and organ movement.

The purpose of this analysis was to determine the extent of OAR movement during simulation and compare it with organ movement during adaptation. Evaluation was performed on the same twenty patients described in the previous section.

All suitable simulation MR images (MRI_{Sim}) of a patient were included in this evaluation to determine the range of organ movement during simulation. Some images had to be excluded, because the breathing phase or patient position were significantly different from the other simulation images. In order to calculate the range of intrafractional OAR movement, both MR images acquired during an adaptive treatment fraction were used. Figure 5 provides an overview of all MR images used for this analysis.

The relevant OARs needed to be completely segmented on all MRI_{Sim}, since the PTV_{Expand} only existed on the MR image of the base plan and could not be used to determine the area in which OARs were contoured. Subsequently, all available simulation MR images were rigidly registered to the MR image of the base plan, using the visible tumor structure. On the basis of this registration, OAR contours were transferred to the MR image of the base plan.

For the adapted fractions, MRI_{pI} was registered to MRI_A using a region of interest (ROI) based registration algorithm. Since the GTV contour was identical in both MR images, it was selected as the relevant ROI for registration. In analogy to the simulation images, the OAR contours from MRI_{pI} (OAR_{pI}) were then transferred to MRI_A, with the result that the OAR contoured on MRI_A (OAR_A) and OAR_{pI} were present on the same MR image. RayStation® 11B (RaySearch Laboratories AB, Stockholm, Sweden) was used for previously described image registration and transfer of contours.

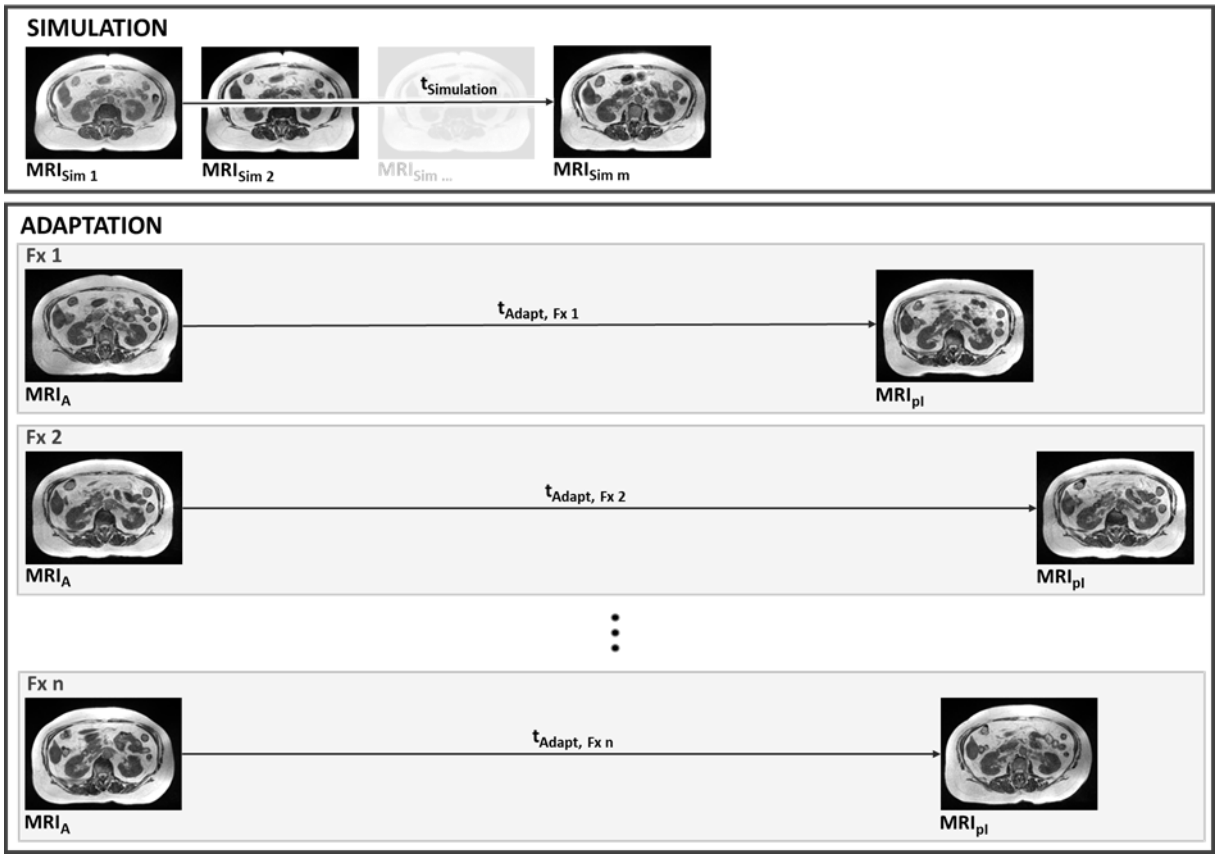

Figure 5: MR images acquired during simulation and adaptation. During simulation at least two images $MRI_{Sim\ 1}$ and $MRI_{Sim\ 2}$ were acquired. For some patients up to m images were available ($MRI_{Sim,\ m}$). At the start of each treatment fraction a MR image was acquired (MRI_A). After adaptation and immediately before irradiation a second image was acquired (MRI_{pI}). The duration between acquisition of the first and last simulation image is labelled $t_{Simulation}$ and the time between MRI_A and MRI_{pI} is labelled as t_{Adapt} and corresponding fraction number. (Buchele et al. 2024)

The following analysis of the extent of OAR movement was performed automatically using a MATLAB script specifically designed for this purpose. Comparable to the dosimetric analysis, this script used the exported DICOM files to reconstruct structures and dose on respective MR images. This was followed by the actual analysis of organ movement. In a first step, the region in which the evaluation of OAR movement was performed was defined. For this purpose, the mean distance of the OAR tolerance isodose to the PTV (d_{TD}) was determined for each adapted plan as well as the base plan. This distance was chosen because only a certain part of the OAR close to the PTV was supposed to be evaluated, in which relevant dose changes leading to tolerance dose violations might occur. The in-plane length of three voxels was added to the mean distance (d_{TD+3V}), so that the evaluated OAR contour was sufficiently large. The OAR was then cropped outside the area defined by isotropic expansion of the PTV by d_{TD+3V}. In case of the adapted fractions, the OAR_A contour was continuously expanded by an isotropic margin until it completely enclosed OAR_{pI}. The margin resulting from this expansion was

identified as the range of the organ movement during adaptation (RoM_{Adapt}). The steps of this analysis and resulting distances are visualized in Figure 6.

To determine the range of organ movement during simulation (RoM_{Sim}), d_{TD} calculated from the base plan was used to define the region outside which OAR contours were cropped. Subsequently, the OAR contour of the first simulation image was expanded until it completely enveloped the OAR contour from a following simulation MR image. If multiple simulation images were available, the range of movement (RoM) was determined between the OAR contours of the first and the last simulation image as well as between contours of successive simulation images. In a further analysis, not only movement towards, but also movement away from the PTV was included in determination of RoM_{Sim}. This was achieved by expanding OAR contours from MR images that were acquired later in the simulation session until they enclosed OAR contours from MR images acquired earlier in the same session. Since several RoM values were calculated when including more than two MRI_{Sim} for analysis, the maximum RoM ($RoM_{Sim,\ max}$) value was determined and used for comparison with the intrafractional organ movement.

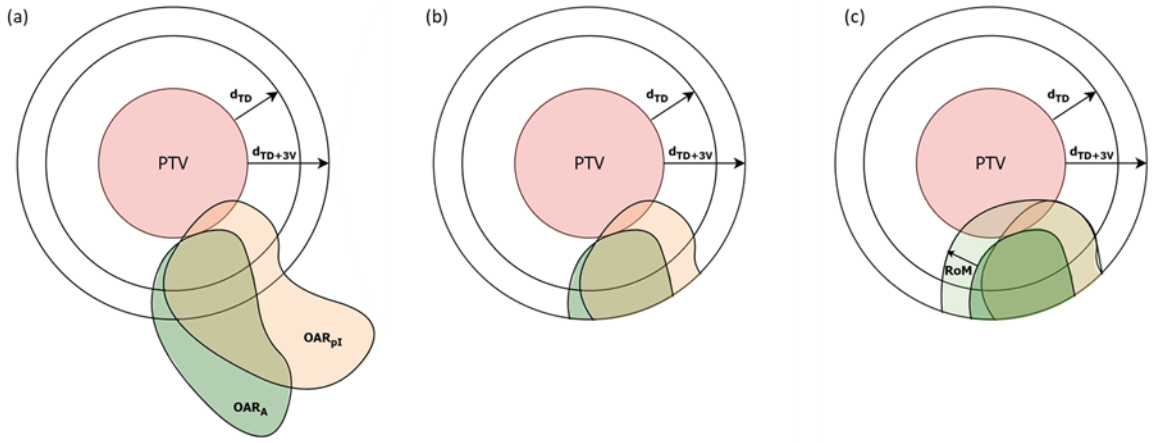

Figure 6: Schematic of the method used to determine range of movement (RoM) of organs at risk including all contours and distances. (a) The mean distance of the OAR tolerance dose from the PTV was determined (d_{TD}) and the in-plane length of three voxels added (d_{TD+3V}). The OAR contour from MRI_{pI} (OAR_{pI}) was transferred to MRI_A, so the OAR from MRI_A (OAR_A) and OAR_{pI} existed in the same image. (b)The OAR contours were cropped inside an area around the PTV expanded by d_{TD+3V}. (c) OAR_A was expanded until it completely enveloped OAR_{pI}. The resulting margin used to expand OAR_A was called RoM. (Buchele et al. 2024)

For each patient, the percentage of adapted fractions was calculated, in which the maximum range of organ movement during simulation was greater or equal to the extent of intrafractional organ movement. This calculation was repeated multiple times using different methods to determine $RoM_{Sim,\ max}$. In a first step, the $RoM_{Sim,\ max}$ value was determined using only the OAR

contour of the first and last simulation image. This was followed by calculation of $RoM_{Sim, max}$ values using all consecutive images including only movement towards the PTV. In a last step, movement away from the PTV was also included. These different methods to calculate $RoM_{Sim, max}$ were established in order to decide, if the predictability of intrafractional OAR movement could be improved by acquisition of multiple MRI_{Sim} and by including all OAR movement detected during simulation.

In addition, a Pearson correlation analysis was used to investigate the correlation between the duration of simulation and the percentage of cases in which RoM_{Sim} is greater than or equal to RoM_{Adapt}. The same type of analysis was employed to evaluate whether duration of simulation sessions had an effect on $RoM_{Sim, max}$ values.

Furthermore, a linear mixed effects model was fit to analyze the relationship between intrafractional changes in OAR dose and the organ movement during adaptation. The dose distribution variant was entered as a fixed effect. Identical to the previous mixed effects models, OAR nested within patient was added as a random intercept:

$$\text{Dose Difference} \sim RoM_{Adapt} + (1 \mid \text{Patient} / \text{OAR})$$

As with the other models no deviations from homoscedasticity or normality were detected.

2.3 Ethics statement

This study was conducted in accordance with the declaration of Helsinki and approved by the local ethics board (Ethikkommission der Medizinischen Fakultät Heidelberg, S-479/2021). Written consent from patients was not necessary in case of this study.

3 RESULTS

3.1 Impact of intrafractional changes on dose to organs at risk

3.1.1 Explorative analysis of a limited number of patients with abdominal lesions

Correlation between the minimal distance between OAR and PTV on MRI_A and the difference between predicted and adapted OAR dose as well as between adapted and pre-irradiation OAR dose was evaluated (Figure 7). Minimal distance on MRI_A was selected for this analysis because two of the three evaluated dose distributions were based on MRI_A.

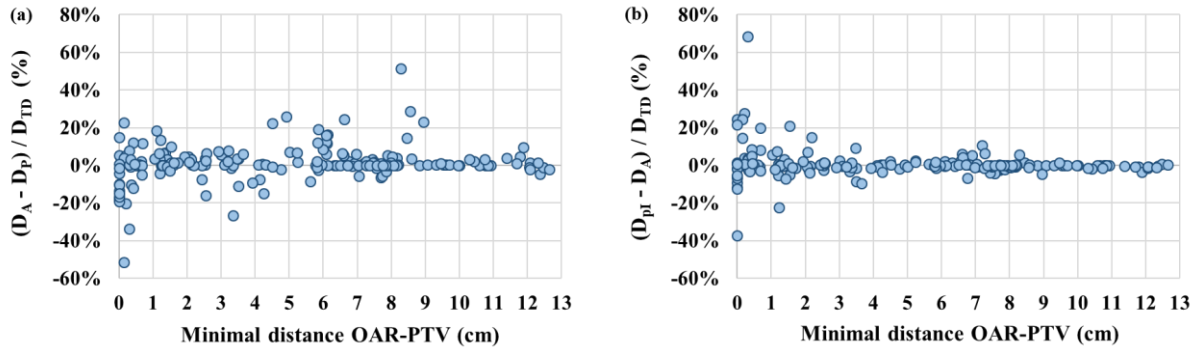

Figure 7: Dose differences relative to OAR tolerance dose plotted over minimal distance between OAR and PTV in MRI_A. (a) Difference between adapted and predicted OAR dose. (b) Difference between pre-irradiation and adapted OAR dose.

Dose differences caused by intrafractional changes were smaller with increasing initial distance between PTV and OAR (Figure 7 (b)). For distances of up to three centimeters, greater variations in dose differences were found with large positive and negative differences of up to 80% of the tolerance dose. Changes of OAR dose with an absolute value over 10% occurred in 13 observations in this distance range, while only one case was detected for distances larger than three centimeters. Three centimeters was chosen to split observations since this distance corresponded to the in-plane margin expansion of the PTV_{Expand}.

Dose differences between predicted and adapted OAR dose showed a similar pattern, with higher variations occurring when the distance between OAR and PTV was smaller (Figure 7 (a)). However, in contrast to the differences between adapt and pre-irradiation variant, there were distinctly more outliers for distances over three centimeters. In this distance range, changes to OAR dose over 10% could be found in sixteen observations. This number was

similar to that of observations with a distance smaller three centimeters, with 18 observations showing dose changes larger than 10%. Furthermore, the magnitude of outlier values was comparable in both distance ranges, with dose differences relative to the tolerance dose of up to 60%. However, outliers in the distance range larger than three centimeters were mainly positive, while they were more evenly distributed between positive and negative values for distances smaller than three centimeters.

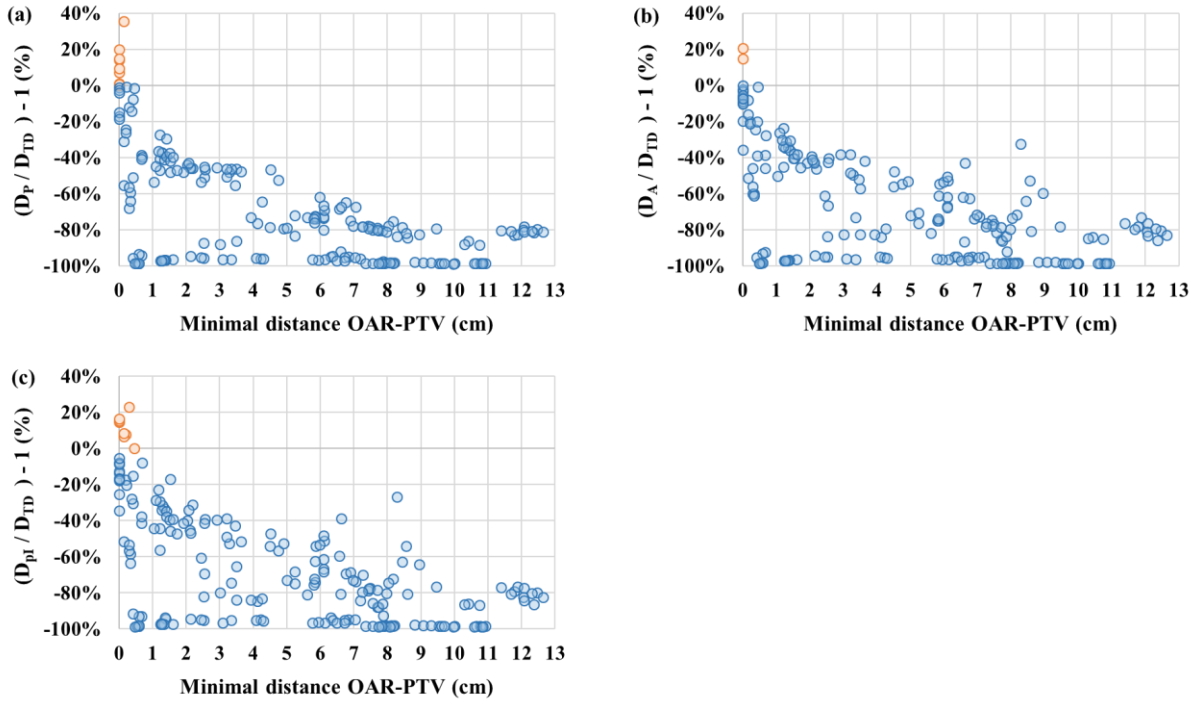

Figure 8: OAR dose relative to tolerance dose plotted over minimal distance between OAR and PTV in MRI_A for predict (a), adapt (b) and pre-irradiation (c) dose distribution variant. Datapoints violating the OAR tolerance dose are plotted in orange, while those meeting the tolerance dose are plotted in blue.

To evaluate the effect of dose changes on the occurrence of OAR tolerance dose violations, the OAR dose of each dose distribution variant was determined and correlation with the minimal distance between OAR and PTV was examined. The results are illustrated in Figure 8. The number of dose constraint violations was reduced from nine violations in the predicted to two violations in the adapted dose distribution variant. Both violations in the adapted variant were caused by incorrect contouring during the original adaptation workflow, once for the heart and once for the right kidney. As a result, the violation of OAR dose could not be detected, and dose could not be sufficiently reduced. Furthermore, OAR dose values were generally higher in the adapted than in the predicted variant if OARs were located farther away from the PTV. However, no violations occurred at these distances.

The number of violations increased again, though, from two in the adapted variant to eight in the pre-irradiation variant. In all of these cases, the OAR was less than a centimeter away from the PTV. OARs that violated the tolerance dose in the pre-irradiation dose distribution variant, were below the tolerance dose in the adapted variant with the exception of one observation, indicating that they were caused by intrafractional changes.

3.1.2 Analysis of patients with abdominal lesions directly next to organs at risk

Results describing differences in OAR dose between adapted and pre-irradiation dose distribution variant as well as analysis of tolerance dose violations in these variants were part of the publication (Buchele et al. 2024).

An overview over OAR dose relative to the tolerance dose for each dose distribution variant can be found in Figure 9. OAR dose increased from predicted to adapted variant in 116 of 189 (61.4%) observations and an increase from adapted to pre-irradiation OAR dose could be observed in 118 of 189 cases (62.4%). To investigate whether the observed changes in OAR dose were significant, linear mixed effect models were fit considering different constellations of dose distribution variants. An analysis of predicted and adapted variants showed that the effect of plan adaptation was statistically non-significant ($p = 0.744$, 95% Confidence Interval (CI) = [-2%, 3%]), even though the model's total explanatory power was substantial ($R^2 = 0.37$). In contrast, the linear mixed effects model using adapted and pre-irradiation dose distribution showed an increase in OAR dose of 4.4% from adapted to pre-irradiation dose. This increase was statistically significant ($p < 0.001$, 95% CI = [2%, 7%]) and the model's total explanatory power was substantial ($R^2 = 0.28$). Similarly, a significant increase in OAR dose of 4.3% between predicted and pre-irradiation was found ($p < 0.001$, 95% CI = [1%, 7%]). As with the other models, this model's explanatory power was substantial ($R^2 = 0.37$).

Additionally, the occurrence of tolerance dose violations in each dose distribution variant as well as changes in the number of violations between variants were analyzed. In the predicted variant OAR tolerance dose was violated in 42 of 189 cases (22.2%). Tolerance dose violations varied between 0.33% and 66.74% (median: 8.24% mm, interquartile range (IQR): 14.36%). The number of violations could be decreased to twelve (6.3%) in the adapted plan with tolerance dose violations ranging between 0.32% and 11.16% (median: 2.21%, IQR: 2.32%). McNemar's test showed that the occurrence of dose constraint violations changed significantly between

predicted and adapted dose distribution ($p < 0.05$). However, in the pre-irradiation variant the number of tolerance dose violations increased again to 60 cases (31.7%). For this variant, tolerance dose violations between 0.04% and 41.9% (median: 5.9%, IQR: 6.99%) were determined. As for predicted and adapted dose distribution variant, the number of OAR dose violations differed significantly in adapted and pre-irradiation variant (McNemar's test, $p < 0.05$).

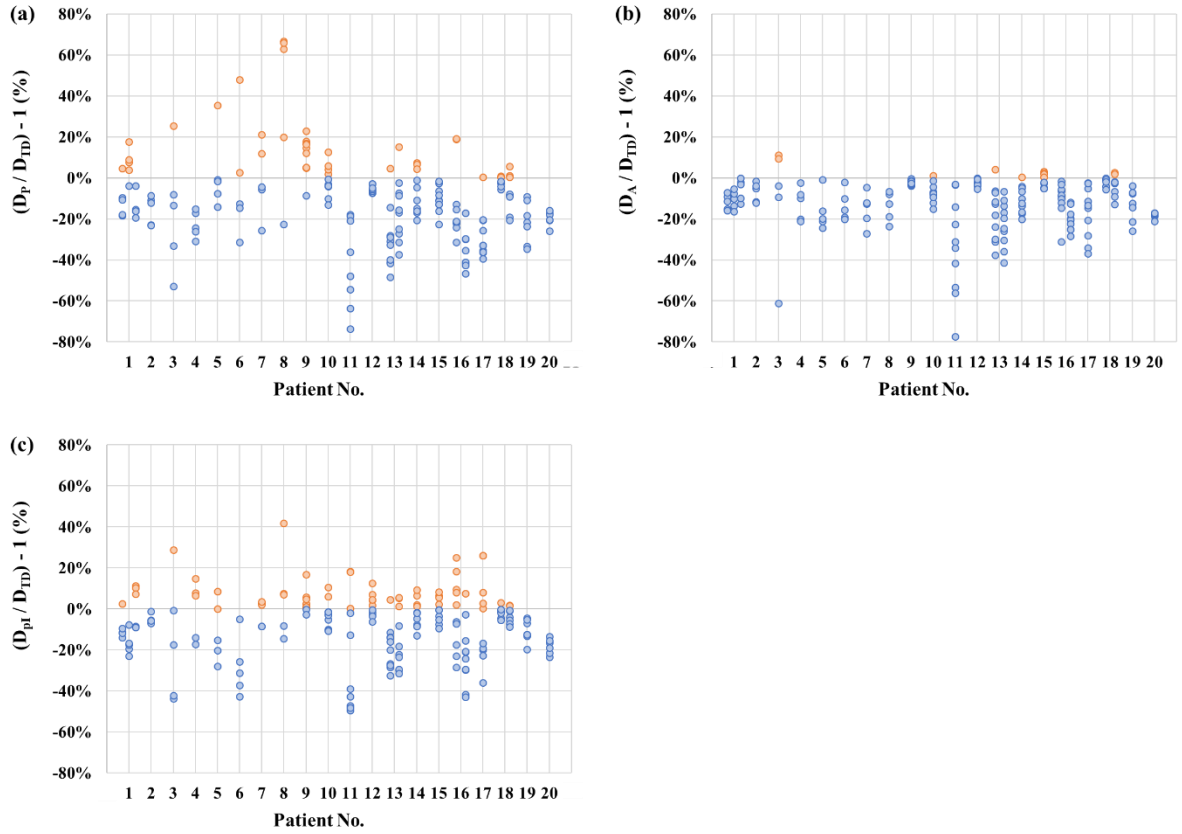

Figure 9: OAR dose relative to tolerance dose for predict (a), adapt (b) and pre-irradiation (c) dose distribution variant, plotted separately for each patient and organ at risk. Violations of OAR dose are plotted in orange, while datapoints meeting the OAR tolerance dose are plotted in blue. Adapted from (Buchele et al. 2024) and expanded to also include OAR dose in the predicted variant.

If tolerance dose violations were regarded separately for each type of OAR, most violations could be observed in the small bowel with 28/100 dose violations in the predicted, 7/100 in the adapted and 34/100 in the pre-irradiation variant. For the duodenum, there were fewer violations in predicted and adapted dose distribution variants with 7/45 and 5/45 violations, respectively, but distinctly more observations violated the tolerance dose in the pre-irradiation variant (18/45 violations). Distinctly less violations were detected in the stomach with 7/39 violations in the predicted, no violations in the adapted and 5/39 violations in the pre-irradiation

dose distribution variant. No violations occurred in the esophagus in either the predicted or the adapted variant, but 3/5 violations were found in the pre-irradiation variant.

Additionally, the occurrence of tolerance dose violations in pre-irradiation dose distribution variant varied strongly between the evaluated patients. Even though the total number of violations was the highest for duodenum, tolerance dose of this OAR was not violated for some patients in any fraction, while for other patients, tolerance dose violations occurred in multiple fractions.

Table 3: Compliance with dose variants in the three dose distribution variants.

Compliance with dose constraints ✓: Constraint met ✗: Constraint violated			Percentage of all observations	Total number of observations
Predict	Adapt	Pre-Irradiation		
✓	✓	✓	53,4%	101
✓	✗	✓	3,2%	6
✗	✓	✗	7,4%	14
✗	✗	✗	1,1%	2
No change (Predict = pre-Irradiation)			∑ 65,1%	∑ 123
Predict	Adapt	Pre-Irradiation		
✗	✓	✓	12,7%	24
✗	✗	✓	0,5%	1
Better compliance with dose constraints			∑ 13,2%	∑ 25
Predict	Adapt	Pre-Irradiation		
✓	✓	✗	19,6%	37
✓	✗	✗	2,1%	4
Worse compliance with dose constraints			∑ 21,7%	∑ 41

Table depicting compliance of the OAR dose in predict, adapt and pre-irradiation dose variant with OAR tolerance dose. The number of observations and percentage of total observations fitting each combination of dose constraint compliance is shown.

Table 3 provides an overview of different combinations of OAR tolerance dose violations in dose distribution variants and the frequency with which each combination occurs. In 63.0% of cases adaptation had no effect on violation of the OAR tolerance dose, which meant that the status of dose violation was the same in predicted and pre-irradiation dose distribution. For most of these cases, OAR tolerance dose was met in all variants (51.9%). In 7.4% of cases OAR dose could be reduced below the tolerance dose, but this effect was negated due to intrafractional changes. Additionally, in 21.2% of observations, violations occurred in the pre-irradiation dose distribution, even though the tolerance dose was met in the adapted as well as in the predicted variant. Adaptation was necessary due to OAR tolerance dose violations in the predicted dose distribution variant in 22.2% of cases and in a majority of these cases (20.6% of all cases) could indeed be reduced below the tolerance dose. However, due to intrafractional changes pre-irradiation dose was violated again in 7.4% of cases.

Analysis of the cause of intrafractional changes showed that differences in OAR dose were induced by organ movement due to peristalsis in 170 of 189 observations. Large variations in stomach filling led to changes between adapted and pre-irradiation OAR dose in 13 observations. In some of these cases not only the stomach was affected, but the duodenum was largely displaced by the stomach emptying into the duodenum. In another six observations matching from MRI_{pI} to MR_A was incorrect. As a consequence, OAR contours on MRI_{pI} were situated inside the GTV, even though they were not part of the GTV on MRI_A.

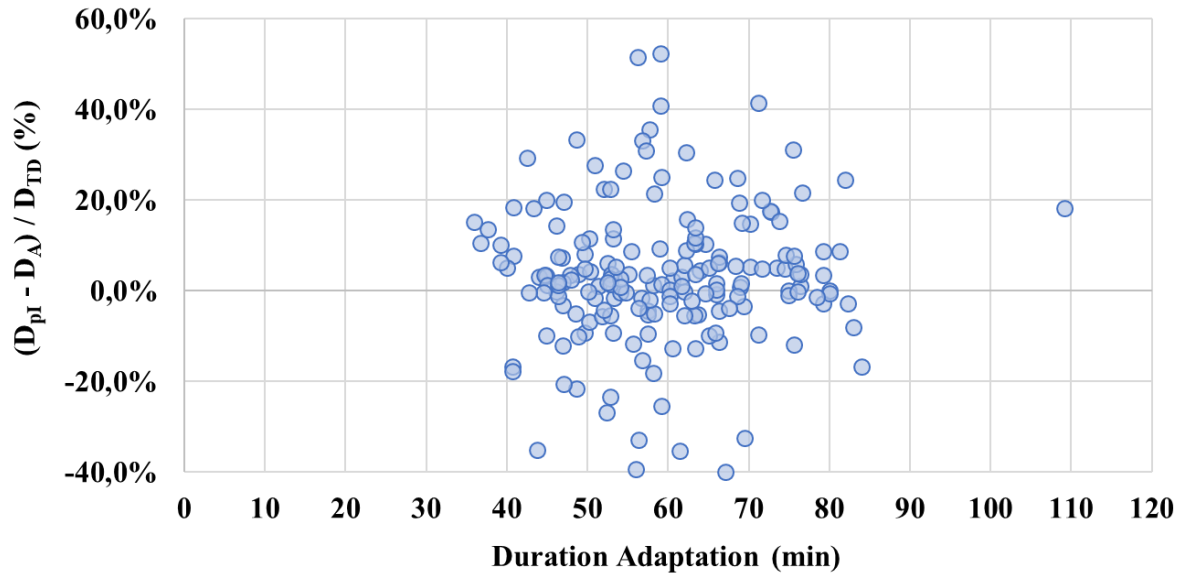

Figure 10: Difference of pre-irradiation and adapted OAR dose plotted over the duration of the adaptation process.

The median time between MRI_A and MRI_{pI} over all patients was 58.1 minutes. Adaptation times varied between 36.0 and 109.2 minutes. A scatterplot with dose difference relative to tolerance dose plotted over the duration of adaptation is depicted in Figure 10. No pattern could be determined in this scatterplot. The fitted linear mixed effects model further showed that the effect of adaptation time on dose change is statistically non-significant ($p = 0.535$, 95% CI = [- 0.1%, 0,3%]). Random effects variances were 0 for this model and therefore no conditional R^2 is available. The marginal R^2 value related to the fixed effects was near zero (0.0021).

3.2 Predictability of organ at risk movement during adaptation

Results on range of organ movement during adaptation were also included in the publication (Buchele et al. 2024). For range of movement during simulation sessions only those methods evaluating organ movement towards the PTV were a part of the publication. Also incorporated in the publication were results of the analysis of agreement between $RoM_{Sim,\ max}$ and RoM_{Adapt} as well as results of the correlation analysis between $RoM_{Sim,\ max}$ and duration of simulation.

The duration of simulation sessions was between 1.6 and 27.9 minutes. Four simulation MR images were acquired for most patients (8/20), followed by two MR images (7/20). For the other patients either three (3/20), six (1/20) or seven simulation MR images (1/20) were available for analysis. For those patients with two simulation images, only one RoM_{Sim} value could be determined.

The range of maximum OAR movement during simulation sessions varied between 4.5 mm and 15.0 mm (median: 7.5 mm, interquartile range (IQR): 3.7 mm, n: 25), when all images were included in the determination of RoM_{Sim} and movements towards and away from the PTV were considered. Slightly lower variations were determined for RoM_{Adapt} values (median: 6.0 mm, IQR: 3.0 mm, n: 187) with values ranging from 1.5 mm to 22.8 mm. However, there were more outliers in RoM_{Adapt} with values of up to 22.8 mm and the extent of variations differed considerably between patients. Some patients showed large variations between lowest and highest RoM_{Adapt} value, for example patient 13 with values between 1.5 mm and 19.6 mm. In other patients, e.g. patient 5, RoM_{Adapt} values only varied slightly between 4.5 mm and 7.5 mm. RoM_{Adapt} could not be determined in two adapted fractions of patient 10 because the OAR was outside the area defined by d_{TD+3V}. Characteristics of the evaluated simulation sessions and the range of RoM_{Sim} and RoM_{Adapt} for each patient can be found in Table 4.

.

Table 4: Overview over simulation image characteristics, OARs and results of RoM analysis.

Patient No.	Duration Simulation (min)	No. of MRI_{Sim}	OAR	Range RoM_{Sim} (mm)	Median RoM_{Adapt} (mm)	Range RoM_{Adapt} (mm)
1	27.0	7	Stomach	4.5 – 10.5	7.5	3.0 – 7.5
		7	Duodenum	3.0 – 6.0	4.5	3.0 – 7.5
		7	Esophagus	4.5 – 7.5	6.0	3.0 – 6.0
2	11.2	2	Small bowel	12.0*	7.5	4.5 – 10.5
3	19.2	4	Small bowel	4.5 – 9.0	9.0	7.5 – 13.5
4	26.9	4	Duodenum	1.5 – 6.0	4.5	1.5 – 13.5
5	27.6	4	Stomach	4.5 – 7.5	6.0	4.5 – 7.5
6	15.2	4	Stomach	4.5 – 15.0	3.0	1.5 – 7.5
7	17.1	3	Duodenum	3.0 – 4.5	4.5	3.0 – 10.5
8	8.0	2	Small bowel	7.5*	9.0	3.0 – 10.5
9	18.6	4	Small bowel	4.9 – 11.4	6.5	4.9 – 9.8
10	28.7	3	Small bowel	4.5 – 7.5	4.5	4.5 – 7.5
11	10.1	4	Small bowel	4.9 – 8.2	10.6	6.5 – 22.8
12	16.2	4	Duodenum	4.5 – 12.0	6.0	4.5 – 9.0
13	5.4	2	Small bowel	6.0*	8.3	4.5 – 13.5
		2	Duodenum	7.5*	5.3	1.5 – 19.6
14	1.6	2	Small bowel	6.0*	8.3	4.5 – 12.0
15	13.5	2	Duodenum	4.5*	4.5	3.0 – 7.5
16	27.9	6	Small bowel	3.0 – 10.5	10.5	3.0 – 15.0
		6	Stomach	3.0 – 6.0	4.5	1.5 – 9.0
17	22.2	3	Small bowel	3.0 – 7.5	5.3	3.0 – 9.0
18	8.5	2	Stomach	4.5*	3.8	3.0 – 7.5
		2	Small bowel	4.5*	3.8	3.0 – 4.5
19	22.8	4	Small bowel	6.0 – 9.0	6.0	3.0 – 13.5
20	7.5	2	Stomach	7.5*	6.8	3.0 – 9.0

Characteristics of analyzed simulation sessions and range of RoM values determined for simulation and adaptation for each patient. Adapted from (Buchele et al. 2024). *No range could be determined since only two images were available for analysis.

Figure 11 depicts $RoM_{Sim,\ max}$ values determined with different methods plotted over the duration of simulation for each evaluated OAR. Large range of OAR movement up to 7.5 mm was determined even for short simulation times below 6 minutes. Similar values could be found for simulation times longer than 25 minutes. Furthermore, Pearson correlation analysis found no significant correlation between duration of the simulation session and $RoM_{Sim,\ max}$ value for either method to determine $RoM_{Sim,\ max}$ ($p > 0.05$), which signifies that for the evaluated patients, shorter simulation time did not lead to lower $RoM_{Sim,\ max}$ values.

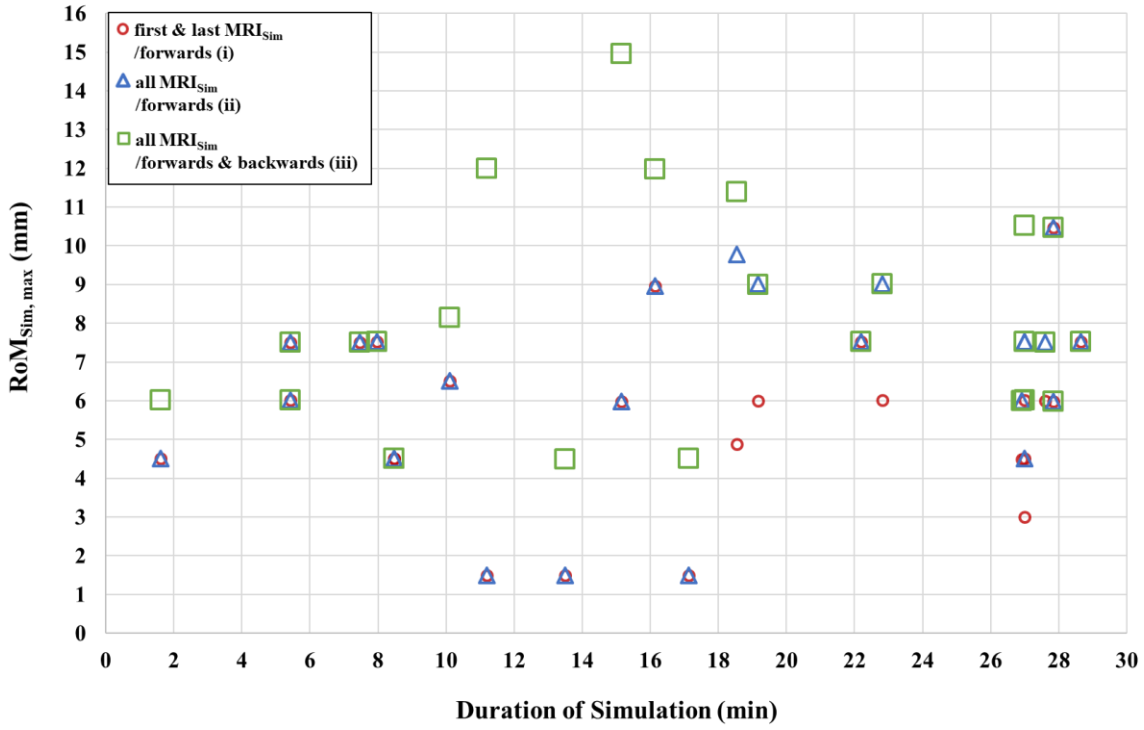

Figure 11: $RoM_{Sim,\ max}$ values plotted over duration of the simulation session. Different methods were applied to calculate $RoM_{Sim,\ max}$. (i) Using only the first and last MRI_{Sim} and considering only movement towards the PTV (ii) Using all MRI_{Sim} and considering only movement towards the PTV. (iii) Using all MRI_{Sim} and including movement towards and away from the PTV.

RoM_{Adapt} values were equal or smaller than $RoM_{Sim,\ max}$ in 104 of 187 observations (55.6%), when only the first and last MR image acquired during simulation were used to determine $RoM_{Sim,\ max}$. By including all images acquired during simulation, this could be increased significantly to 126 observations (67.3%). If in addition to movement towards the PTV, OAR movement away from the PTV was included in determination of $RoM_{Sim,\ max}$, the number of fractions with RoM_{Adapt} smaller or equal to $RoM_{Sim,\ max}$ could be further increased to 144 observations (77.0%). However, the number of observations where $RoM_{Sim,\ max}$ was distinctly higher than RoM_{Adapt} increased when using this method.

Figure 12 illustrates these findings. A frequency distribution of the differences between RoM_{Adapt} and $RoM_{Sim,\ max}$ using the three different methods to identify $RoM_{Sim,\ max}$ is depicted. A negative value signifies that $RoM_{Sim,\ max}$ was larger than RoM_{Adapt} for this specific observation. Both frequency distributions of those methods that included all MRI_{Sim} to determine RoM_{Sim} are shifted in a negative direction compared to the method using only the first and last simulation image. However, RoM_{Adapt} is overestimated by 4.95 mm or more with an even higher frequency in case OAR movement towards and away from the PTV was included to determine $RoM_{Sim,\ max}$. All negative difference values smaller than -9.9 mm can be attributed to patient 6 for whom a high $RoM_{Sim,\ max}$ value of 15 mm was determined.

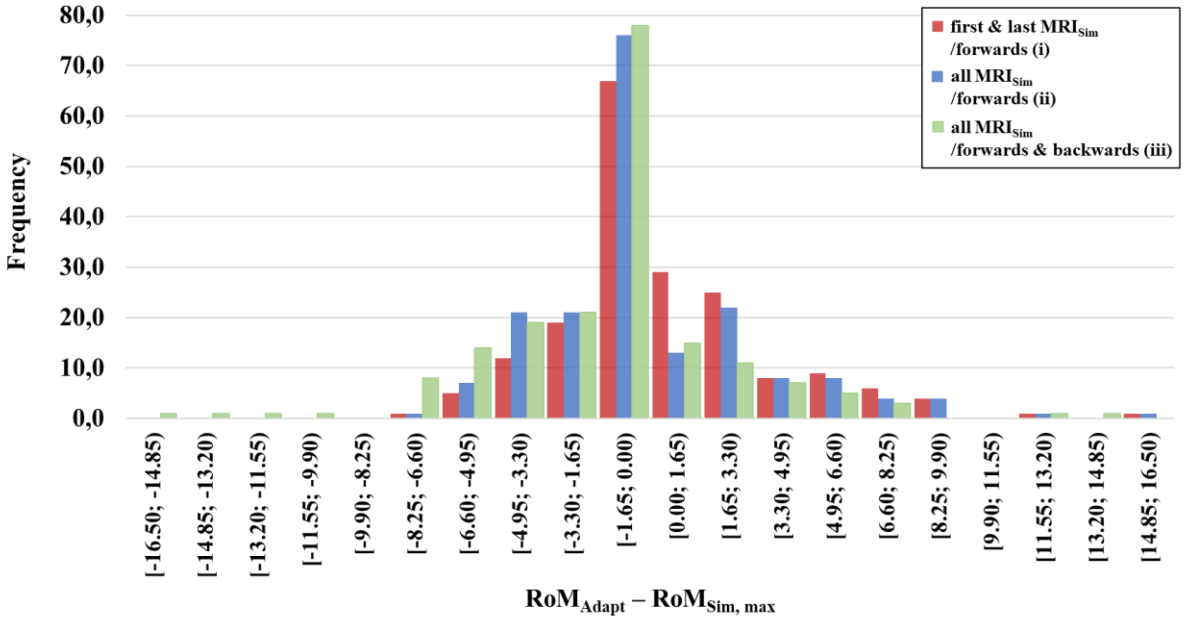

Figure 12: Frequency distribution of differences between RoM_{Adapt} and $RoM_{Sim,\ max}$ using different methods to define $RoM_{Sim,\ max}$. Range of movement during simulation was determined using the first and last MRI_{Sim} (i) and using all MRI_{Sim} (ii), in both cases only including movement towards the PTV (termed forwards). The third method (iii) used all simulation images, while additionally considering movement away from the PTV (termed backwards). Bin size was 1.65 mm, since differences are a multiple of image voxel size and voxel sizes were between 1.48 mm and 1.63 mm.

Furthermore, the correlation between duration of simulation sessions and the percentage of fractions, where $RoM_{Sim,\ max}$ is greater or equal to RoM_{Adapt} was analyzed (Figure 13). There was no significant correlation if $RoM_{Sim,\ max}$ was calculated using the first and last MRI_{Sim} (Pearson correlation coefficient: 0.22, $p > 0.05$). Both other methods to determine $RoM_{Sim,\ max}$ showed a significant correlation, though. Correlation coefficients were 0.52 ($p < 0.05$) for the method using all MRI_{Sim} and forwards movement, and 0.53 ($p < 0.05$) using all MRI_{Sim} and forwards as well as backwards motion of OARs. This implies that $RoM_{Sim,\ max}$ coincided better

with RoM_{Adapt} if simulation sessions were longer and if multiple images were acquired during simulation.

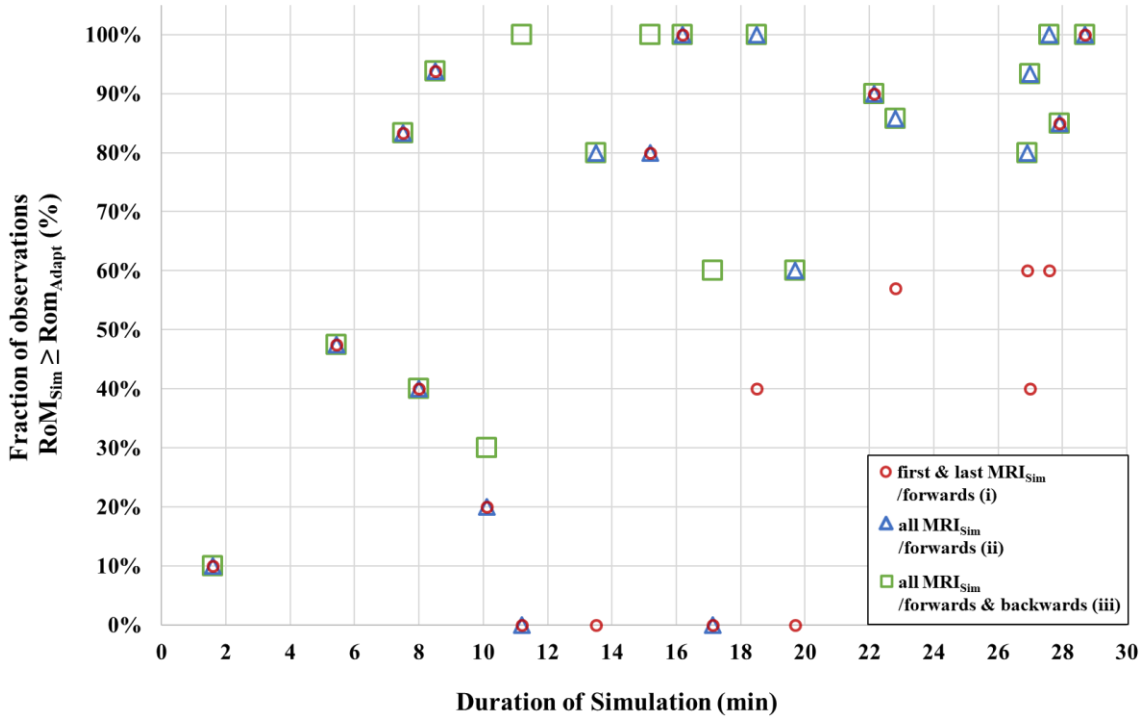

Figure 13: For each patient, the percentage of fractions with $RoM_{Sim,\ max}$ equal or larger than RoM_{Adapt} was plotted over duration of the simulation session. Multiple OARs in one patient were combined to one datapoint. Different methods were used to calculate $RoM_{Sim,\ max}$. (i) Determination of $RoM_{Sim,\ max}$ using only the first and last MRI_{Sim} and considering only movement towards the PTV (ii) Determination of $RoM_{Sim,\ max}$ by including all MRI_{Sim} and considering only movement towards the PTV. (iii) Determination of $RoM_{Sim,\ max}$ using all MRI_{Sim} and including movement towards and away from the PTV.

To further evaluate the effect of simulation time on agreement between $RoM_{Sim,\ max}$ and RoM_{Adapt}, observations were separated by duration of the simulation. The median duration of simulation sessions of all patients was 17.1 minutes and therefore this value was chosen to split observations. For those patients with simulations sessions longer than 17.1 minutes, RoM_{Sim} was equal or larger than RoM_{Adapt} in 89.7% of observations when using all images and only forward movement to determine RoM_{Sim}. The same percentage was found, when movement away from the PTV was additionally considered for the definition of RoM_{Sim}. For simulation sessions below 17.1 minutes, RoM_{Sim} coincided with RoM_{Adapt} in only 56.0% of observations using all simulation MR images and only motion toward the PTV. In contrast to simulation times over 17.1 minutes, the percentage of observations increased distinctly to 66.3% by including movement away from the PTV for determination of the maximum RoM_{Sim} value.

Additionally, the effect of organ movement on the difference between adapted and pre-irradiation OAR dose was investigated. A linear mixed effects model was fit to analyze the data. The results showed dose differences increased by 2.2% on average for each millimeter that RoM_{Adapt} was higher ($p < 0.001$, 95% CI = [(2%, 3%)]). Marginal R^2 related to the fixed effects was 0.2. No conditional R^2 was available since the estimated variance of random effects was 0. The determined organ movement was higher than 3 mm in most cases. Only seven observations had smaller RoM_{Adapt} values, which were all associated with a lower pre-irradiation OAR dose compared to the adapted dose distribution. RoM_{Adapt} values of 0 meant that the pre-irradiation OAR contour was smaller than the adapted contour in the evaluated area therefore farther away from the PTV. Visual inspection of those cases with RoM_{Adapt} values of 1.5 mm showed that only a small difference in OAR contours were present at the edge of the evaluated area and farther away from the PTV. Positive dose changes occurred above organ movement of 3 mm, and motion over 4.5 mm was already associated with a possible increase in OAR dose over 10%. However, for organ movement up to 12 mm not only positive but also negative dose changes were observed.

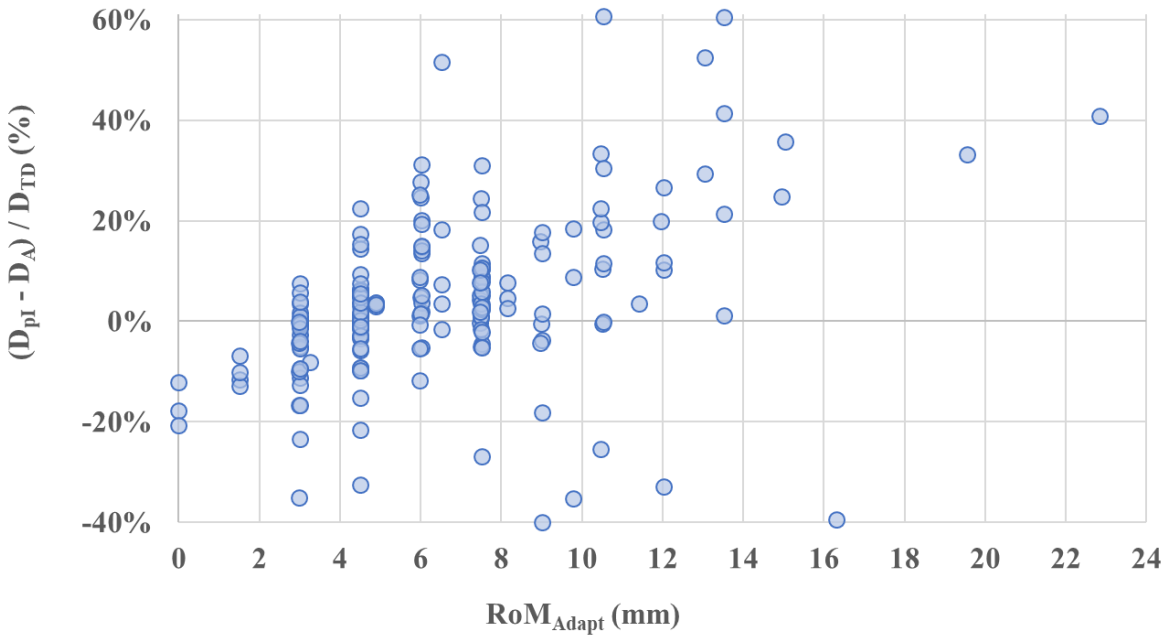

Figure 14: Difference between pre-irradiation and adapted OAR dose relative to the tolerance dose plotted over respective RoM_{Adapt} values for each observation.

4 DISCUSSION

Based on the previously presented results, the three hypotheses defined in the introduction will be examined. In a first step, theses hypotheses will be evaluated separately and afterwards a joint conclusion will be presented.

Some parts of the following discussion, which involve the effects of intrafractional dose changes and the predictability of organ movement during adaptation by using simulation MR images, were covered in the previously mentioned publication (Buchele et al. 2024). This includes possible implications for OAR dose constraints, the possibility of creating PRVs, as well as the possible effects of a shortened adaptation time.

4.1 Hypothesis - “For some cases, adaptation has no benefit”

Evaluation of dose changes in organs at risk caused by adaptation as well as dosimetric changes occurring during the adaptation process mainly support the hypothesis that in some cases, adaptation has no benefit for the patient. In the preliminary analysis with five patients, organs with some distance to the PTV presented with higher dose after plan adaptation. For the evaluated patient plans, no optimization objective was used on OARs that were not directly next to the PTV, since the manufacturer initially recommended to use as few objectives as possible. Therefore, after the introduction of MR-guided adaptive treatment in Heidelberg, most patient plans only included objectives for the PTV, a general normal tissue objective and an additional objective for OARs directly next to the PTV. As a result, different beam angles were used preferentially in the adapted plan compared to the base plan, which caused a higher dose in OARs in some adapted fractions.

Moreover, an increase in OAR dose in adapted fractions could also be found for organs close to the PTV. In the analysis of patients with OARs close to the PTV an increase between predicted and adapted OAR dose was found in a majority of cases. One possible reason for this increase might be a different relative position of the OAR closer to the PTV compared to the base plan. In order to achieve a good PTV coverage, OAR dose needed to be increased when reoptimizing the base plan during adaptation. Furthermore, optimization objectives might have been less effective if the OAR was situated farther away from the PTV compared to the base plan. Usually, dose thresholds of these optimization objectives are defined in the base plan. As

a result, they might not prevent an increase from predicted to adapted OAR dose during reoptimization if the predicted OAR dose was already lower than the objective's dose threshold and no adjustments to the threshold were made. An overview over changes that might occur due to plan adaptation is shown in Figure 15 including reduction of OAR dose due to a tolerance dose violation, increase in OAR dose due to a missing optimization objective and aforementioned change of OAR position relative to the PTV.

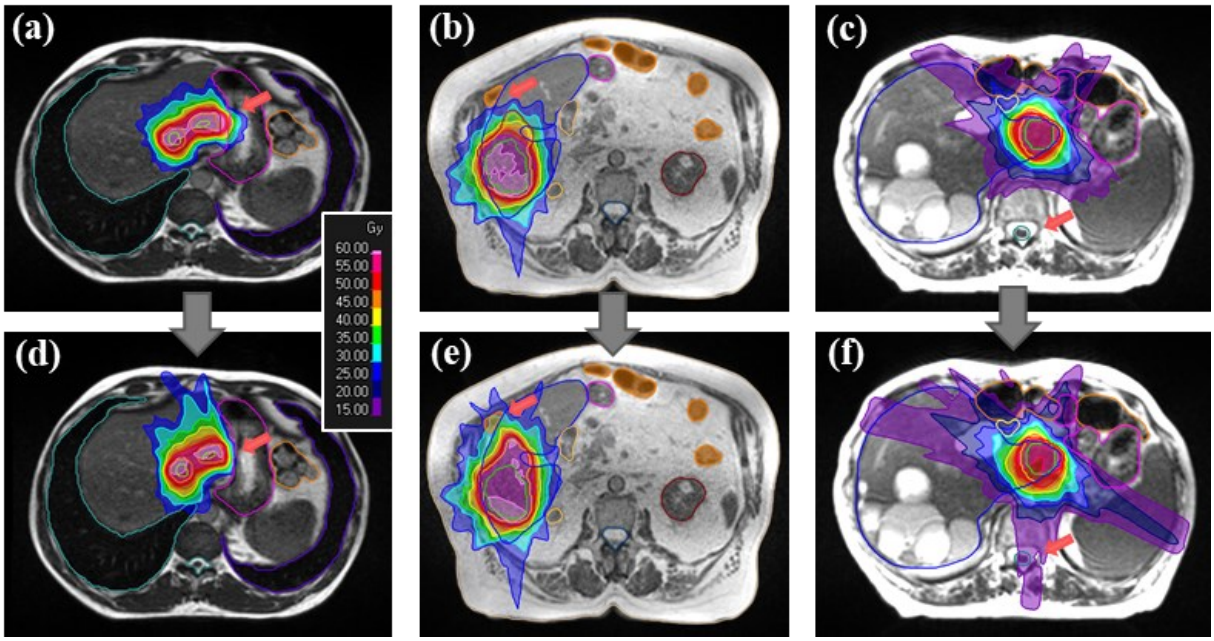

Figure 15: Overview of changes in OAR dose that might occur due to adaptation. The upper row shows the predicted dose distribution variant and the lower row corresponding adapted dose distribution variant. Images (a) and (d) show dose reduction in the stomach close to the PTV since the tolerance dose was violated in the predicted variant. Images (b) an (d) show that dose in the small bowel needed to be increased in order to achieve a good PTV coverage. This was necessary since relative position of small bowel and treated lesion changed compared to the base plan. Images (c) and (f) depict an increase in spinal cord dose from predicted to adapted variants due to a missing optimization objective.

Additionally, the benefit gained by adaptation was mitigated in a significant fraction of patient treatments due to intrafractional changes. Intrafractional organ movement could lead to an increase in organ dose and a subsequent violation of tolerance doses in OARs close to the PTV. This was first detected in the preliminary analysis with five patients, where an increase in the number of violations from the adapted to the pre-irradiation dose distribution variant was observed. All of these violations occurred in OARs that were located less than 1 cm away from the PTV. As a result of these findings, the second evaluation with twenty patients was focused on dose changes in organs directly next to the target volume. In this analysis, a significant increase in overall OAR dose was found between adapted and pre-irradiation dose distribution. As a consequence, the number of tolerance dose violations also increased significantly between

both variants, which was similar to the preliminary analysis. However, the increase in OAR dose did probably not lead to constraint violations in all cases, because intrafractional changes in OAR position were not large enough to cause a violation. In other cases, the OAR was initially far away from the PTV, so even larger changes in OAR position did not lead to a dose constraint violation (Figure 16).

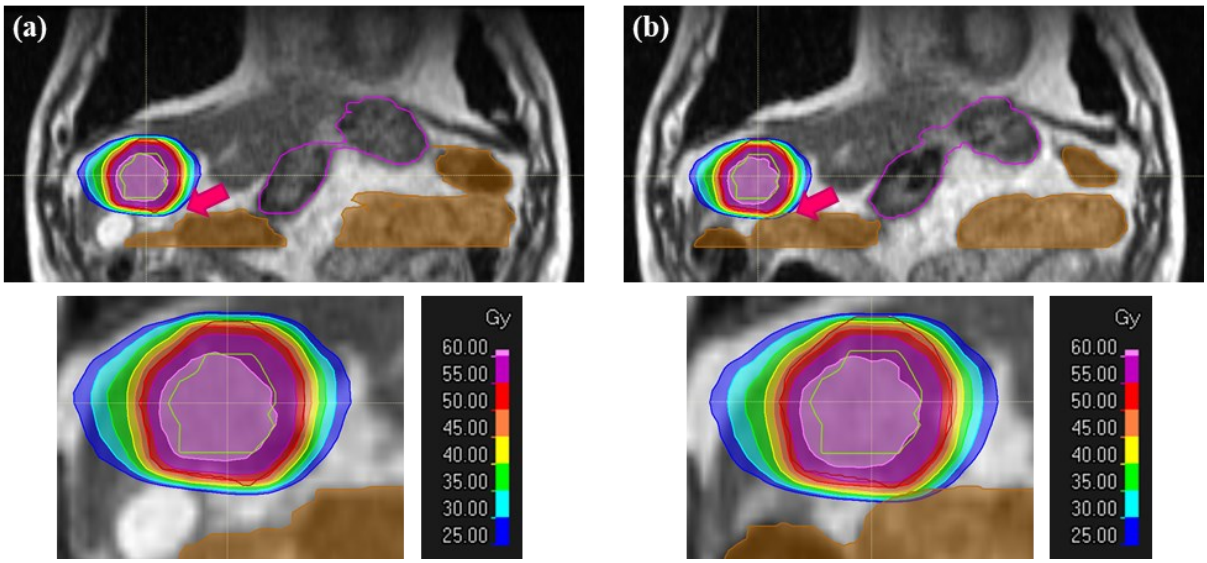

Figure 16: Example of one fraction where small bowel dose increased from adapted (a) to pre-irradiation (b) dose distribution variant due to OAR moving closer to the PTV. However, OAR tolerance dose was not violated since the OAR was still far enough from the PTV. Small bowel is depicted in brown, stomach in pink, GTV in green and PTV in red.

Furthermore, an analysis of the reasons for main anatomical differences revealed that not all dose constraint violations could be attributed to organ movement like peristalsis or gastric contraction. Some were caused by incorrect matching of MRI_{pI} to MRI_{A}, which led to the OAR contour overlapping with the GTV contour even though it was not a part of the GTV. In other cases, intrafractional dose changes could be attributed to the stomach being filled at the start of adaptation and emptying during the adaptation process.

Although there was no significant change of OAR dose between predicted and adapted dose distribution variants, the number of tolerance dose violations could be decreased significantly. Some violations still occurred in the adapted plan because OAR dose could not be reduced below the tolerance dose due to an unfavorable anatomy of the day. Thus, a higher OAR dose was accepted for single fractions of patient treatment. Another reason for dose violations in the adapted plan was slightly incorrect recontouring of OARs during the adaptive workflow that

went undetected. Therefore, OAR dose was violated in dose distribution variants with recontoured organs, even though tolerance dose seemed to be met during the initial adaptation.

In a majority of those cases where OAR dose could be sufficiently reduced through adaptation it also remained below the tolerance dose in the pre-irradiation version. In addition, the magnitude of dose violations in the pre-irradiation variant was lower compared to violations in the predicted variant, which indicates that adaptation had at least some effect on OAR dose by preventing doses that were distinctly higher than the tolerance dose. Furthermore, in a majority of cases no change regarding OAR tolerance dose violations was found, meaning that OAR tolerance dose was met in all dose distribution variants. This suggests that adaptation was performed to increase PTV coverage in these cases while OAR dose could be maintained below the tolerance dose threshold.

Most research on the benefit of adaptive MR-guided radiotherapy is focused on organs close to the PTV since violations of OAR tolerance dose primarily occur in high dose areas. Therefore, only few data are available on the effects of adaptation on dose to organs with some distance to the PTV. Regnery at al. found increased OAR dose in organs with some distance to the PTV in the accumulated dose compared to the base plan (Regnery et al. 2023). Especially in the spinal cord, significant dose increases of up to 9 Gy (equivalent dose in 2 Gy fraction) were found. This supports the findings of the analysis with a limited number of patients and further indicates that the increase in OAR dose found in single fractions could be relevant for the whole patient treatment.

The benefit of adaptation to reduce the number of OAR tolerance dose violations has already been described extensively in previous studies for various abdominal lesions, which is in accordance with the results of this study. Henke et al. reported that in treatments of abdominal lesions the number of tolerance dose violations, which were the main reason for adapting the treatment plan, could be reduced to zero in the adapted plan (Henke et al. 2018a). For the treatment of adrenal metastases, Palacios et al. showed that OAR sparing could be reduced significantly, while reducing the percentage of tolerance dose violations from 27% to 4% in stomach, from 13% to 0% in the bowel and from 3% to 0% in the duodenum (Palacios et al. 2018). Other studies on MR-guided radiotherapy treatments of adrenal metastases (Hoegen et al. 2023), liver metastases (Weykamp et al. 2022), lymphatic oligometastases (Regnery et al. 2022a) and pancreatic cancer (Bohoudi et al. 2019; Michalet et al. 2022b) further confirmed these findings.

However, results on the effect of adaptation on overall OAR doses differ distinctly depending on the study. Some studies found a significantly lower overall OAR dose in organs close to the PTV after plan adaptation in addition to the reduced number of tolerance dose violation. For treatments of the pancreas, Nierer et al. determined a reduction of OAR doses in more than 75% of evaluated cases with a median reduction of 87% (Nierer et al. 2022). In the same study, median and mean dose increased in bowel, duodenum and stomach were found for lesions located in the liver, though. Regnery et al. also reported higher doses in OARs close to the PTV in some patients, when accumulating the doses of adapted plans (Regnery et al. 2023). In this study (chapter 3.1.2) a higher dose after adaptation was found in most cases, but overall, no statistically significant changes between predicted and adapted OAR dose was found.

Research on intrafractional changes during MR-guided radiotherapy is limited so far and a varying impact on the adaptation result is reported. Most studies agree, though, that intrafractional organ movement could lead to an increase in OAR dose and as a consequence to violations of the respective tolerance dose. An increase in OAR tolerance dose violations due to intrafractional changes was observed in studies by Henke et al. and Teoh et al. (Henke et al. 2018b; Teoh et al. 2022). However, the observed number of tolerance dose violations caused by intrafractional changes was still smaller than in the predicted dose distribution. Additionally, Henke et al. only found violations in small bowel and duodenum, but none in the stomach. For small bowel, a significant increase in organ dose by 4.88 Gy due to intrafractional motion was also reported by Wittman et al., while no significant increase was determined for duodenum, stomach and large bowel (Wittman et al. 2021). In contrast to the previously presented studies, tolerance dose violations were found for all organs at risk in this analysis including duodenum and stomach, although the number of violations for the stomach were distinctly smaller than for the other OARs. Furthermore, the determined number of violations in the pre-irradiation dose distribution is similar to those reported by Teoh et al. with 37%. Distinctly less violations occurred in the predicted dose distribution with 21.7% in this study compared to 73% found by Teoh et al. A higher number of tolerance dose violations for small bowel and a combined structure for stomach and duodenum caused by intrafractional organ movement was determined by Tyagi at al. (Tyagi et al. 2021). OAR doses were determined propagating the adapted plan on MR images at the start of adaptation, before irradiation and after treatment delivery. For the stomach and duodenum structure 21/50 and 27/50 violations were determined on MR images before and after treatment delivery, respectively, while no violations occurred on the first MR

image. Small bowel violated the tolerance dose in 26/50 cases on both images, again with no violations occurring on the image acquired at the start of adaptation. However, comparison to the aforementioned studies proved to be difficult, since in some cases different volume constraints were used to determine the near-maximum point dose. For instance, Tyagi et al used a volume of 0.035 cm^3 in contrast to a volume of 0.5 cm^3 used in this study. Additionally, no exact information on the location of OARs relative to the PTV is available in most studies, which might affect the observed impact of intrafractional movement on tolerance dose violations.

The previously presented results as well as already existing studies show that there are some cases where adaptation has no dosimetric benefit for organs at risk. A higher dose after adaptation was observed in OARs close to the PTV as well as in those farther away, which was also confirmed by previously published studies. As a consequence of these findings, optimization objectives have been introduced for some OARs that are located with some distance to the PTV, although it was against the initial recommendation of the manufacturer to use as few optimization objectives as possible. One major limitation of this practice is, though, that organs are only recontoured inside the PTV_{Expand} area during adaptation. Therefore, optimization objectives mainly work for those OARs with some distance to the PTV, that show limited mobility and do not require much recontouring, e.g. the spinal cord.

For OARs close to the PTV, it might not always be possible to reduce or even maintain the same organ dose as in the base plan through adaptation. Since the anatomy of the day differs considerably from the location of OARs and PTV relative to each other in the base plan in some cases, an increase in OAR dose might be necessary in order to achieve an optimal PTV coverage. Even though tolerance doses are typically met in the scenarios described above, an increase in OAR dose might become relevant, when the patient is supposed to receive a radiotherapy treatment again. Re-irradiation has continuously become more relevant in radiotherapy and an increasing number of patients receives radiotherapy treatments more than once (Andratschke et al. 2022; Nieder et al. 2013). If higher organ doses in adapted plans are not considered in repeated treatments of a patient, it might subsequently lead to violations of tolerance doses and, as a consequence, toxicities in affected OARs might occur. In the future, dose accumulation strategies for adapted treatments might be available and facilitate the detectability of higher organ doses. Although there is some research on dose accumulation

strategies in MR-guided radiotherapy (McDonald et al. 2022; Regnery et al. 2023), there are no commercial solutions available so far and dose accumulation is not routinely performed.

Additionally, intrafractional changes can also lead to higher doses in OARs close to the PTV and a subsequent violation of respective tolerance doses. While the majority of intrafractional OAR dose changes was caused by organ movement including peristalsis and stomach contractions, some of these changes originated from incorrect matching of MRI_{pI} to MRI_{A}. This led to the OAR contour overlapping with the GTV contour even though it was not a part of the GTV. One possible reason might be the limitation of the treatment couch to only move in translational directions. As a consequence, the patient position cannot be corrected adequately if the patient is rotated and correction only in translational directions might lead to incorrect matching of MR images. These cases might be prevented in the future by putting a special focus on OARs close to the PTV when matching MRI_{pI} to MRI_{A}, especially if rotations in patient position are detected. Currently, the main focus of matching is the visible GTV structure and as a result slightly incorrect matching leading to an overlap of GTV and OAR might not be detected in every case. Furthermore, in some cases dose changes could be attributed to the stomach being filled at the start of adaptation and emptying during the adaptation process. As a result, large displacements of the stomach as well as the duodenum were observed. Although all patients were given instructions to arrive to treatment with an empty stomach, a full stomach could still be found in some patients. In the future, these cases might be prevented by consequently treating patients with target volumes close to the stomach or duodenum only with an empty stomach. If treatment is not possible otherwise due to low patient compliance, special care should be taken when reviewing the MR image immediately before treatment in order to detect displacements of OARs caused by the stomach emptying during the adaptation process. Since pre-irradiation dose distributions are not routinely created, a possibly higher OAR dose should be documented and considered for re-irradiation scenarios comparable to higher doses due to adaptation.

Even though adaptation seems to have no dosimetric benefit for OARs in some patients and organ tolerance doses are regularly violated as a consequence of intrafractional changes, OAR toxicities in MR-guided radiotherapy are relatively low. At Heidelberg University Hospital no ≥ 3 grade toxicities of gastrointestinal OARs were reported in adaptive MRgRT treatments of abdominal lesions (Hoegen et al. 2023; Regnery et al. 2022a; Weykamp et al. 2023). Similarly, only a limited number of higher grade or no toxicities at all were observed at other sites in

studies on adaptive MR-guided treatments of pancreas (Bordeau et al. 2022; Eijkelenkamp et al. 2023; Rudra et al. 2019), adrenal metastases (Michalet et al. 2022a; Schneiders et al. 2023), liver tumors (Rogowski et al. 2021) or other abdominal malignancies (Henke et al. 2018a). As an example, Bordeau et al. did not find any higher grade (≥ 3) acute toxicities of the gastrointestinal tract in treatments of pancreatic tumors with a dose of 50 Gy in 5 fractions and only a small percentage of patients developed higher grade late toxicities (Bordeau et al. 2022). Furthermore, in patients treated for adrenal metastases with 35 – 50 Gy in three to five fractions, no severe acute and late toxicities (grade ≥ 3) were observed by Michalet et al., either (Michalet et al. 2022a).

Although these treatments were probably also affected by intrafractional changes in OARs and tolerance dose violations, the low occurrence of severe toxicities indicate that actual organ tolerance doses could be higher than previously presumed. Retrospective observational studies on conventional linear accelerators without daily plan adaptation and beam gating were often used to determine OAR tolerance doses in stereotactic treatments (Benedict et al. 2010; Hanna et al. 2018; Holyoake et al. 2021). These tolerance doses were then adopted for adaptive MR-guided radiotherapy treatments due to the initial lack of specific constraints. In order to define specific organ tolerance doses for adaptive MRgRT, prospective studies are necessary in the future. Higher tolerance doses might also be beneficial for target volume coverage, since the coverage needs to be reduced frequently in current treatments to prevent dose violations of OARs directly next to the PTV. In this case, however, intrafractional changes could become more relevant, as higher OAR dose would be permitted. A further escalation of tumor doses could additionally increase the significance of intrafractional organ movement, even if OAR toxicity seems to be low for current dose prescription schemes. Some dose escalation trials for abdominal lesions are already in progress. In a study on adaptive MR-guided radiotherapy treatments for locally advanced pancreatic cancer a dose of 50 Gy is applied in five fractions and the occurrence of severe gastrointestinal toxicities (grade ≥ 3) is evaluated (Parikh et al. 2018). Furthermore, dose escalation in treatments of primary or secondary liver metastases is assessed in the phase II RASTAF trial. A dose of 50 Gy in five fractions is prescribed to lesions close to OARs, while higher doses of 60 Gy in six fractions are reserved for lesions far from any OARs (Rouffiac Thouant and Rederstorff 2020).

In order to mitigate the dosimetric impact of intrafractional changes and achieve a more robust adaptation result through application of patient-specific PRVs, OAR movement needs to be known before the first adaptive movement. One possibility to determine the extent of intrafraction organ movement using simulation MR images is discussed in the following chapter.

4.2 Hypothesis – "More robust adaptive treatments can be obtained by predicting the extent of intrafractional organ movement before the first treatment"

The analysis of the range of organ movement during simulation and adaptation indicates that the extent of intrafraction organ movement could in fact be determined before the first treatment fraction. In three thirds of the evaluated cases, there was a good agreement between range of movement during simulation and adaptation. Agreement between the maximum organ movement during simulation and adaptation was particularly high if several MR images were acquired during simulation and if simulation sessions lasted longer than 17 minutes. For some patients, coincidence between RoM_{Sim} and RoM_{Adapt} could be further improved by including movement away from the PTV in addition to movement towards the PTV. At the same time this led to overestimation of the range of movement during adaptation in a larger number of cases. However, most cases in which RoM_{Adapt} was largely overestimated by RoM_{Sim} could be attributed to one single patient. This patient had a full stomach at the start of the simulation session, which was continuously emptying during simulation and therefore caused large displacements of organs at risk.

In addition, particularly large amplitudes of OAR movement during adapted fractions led to a lower agreement between RoM_{Sim} and RoM_{Adapt}, since they could not be predicted in most patients regardless of the method used to determine RoM_{Sim}. Some organs at risk showed large organ movement in single fractions with maximum values of up to 22.8 mm found in small bowel, 19.6 mm in duodenum and 9.0 mm in stomach, although the detected range of organ movement during simulation was distinctly smaller.

Calculated RoM_{Adapt} values are comparable to displacements found in previous studies applying different methods to calculate OAR positional changes, which indicates that the proposed margin-based method is indeed suitable to determine positional changes of OARs. Alam et al. found maximum deformations of 22.6 mm for a combined structure of stomach and duodenum and 37.8 mm for small bowel in MR-guided treatments of locally advanced pancreatic cancer (Alam et al. 2022). The reported small bowel displacement was possibly higher than the maximum RoM_{Adapt} value found in this study because a larger part of OAR contours was used to determine displacements and therefore large positional changes in small bowel position did not necessarily occur near the treated lesion.

Uchinami et al. determined an organ-specific margin for compensation of OAR movement using data of multiple CT images acquired for treatment planning (Uchinami et al. 2023). The applied method was similar to the one used to calculate RoM values. Median organ-specific margins were 10 mm, 8 mm and 14 mm for stomach, duodenum and intestine, respectively. Since organ-specific median margins were determined in contrast to patient-specific RoM values in this study, a direct comparison was difficult. However, the median patient-specific RoM values range between 3.0 mm and 7.5 mm for the stomach, between 4.5 mm and 6.0 mm for the duodenum and between 3.8 and 10.6 for small bowel and therefore appear to be lower than the values determined by Uchinami et al. As in the previous study by Alam et al, the entire organ structure was used to determine the margins, though, which might have led to higher margins compared to the RoM_{Adapt} values. In addition, only 2 mm step sizes were used to approximate the appropriate margin, which was also slightly higher than the voxel-wise expansion step sizes in this study, which was 1.5 mm for most of the evaluated patients. Other research found organ movements up to 34 mm in the stomach and duodenum and up to 48 mm in the intestine. However, a comparison with the RoM_{Adapt} values proves to be difficult because either organ movement due to peristalsis was not considered separately from other movements like respiration (Zhang et al. 2023) or organ movements were calculated separately for each spatial direction with no overall movement vector being defined (Mostafaei et al. 2018).

Overall, the results of the organ movement analysis show that it can be possible to determine the extent of organ movement before the first adaptive treatment. For some patients with especially large OAR movement during adaptation, agreement between $RoM_{Sim,\ max}$ and RoM_{Adapt} values might be improved, though, by instructing the patient to arrive to every appointment with an empty stomach and by carefully monitoring gastric filling on acquired MR images. Similar to the dosimetric analysis, the results of the RoM evaluation were negatively influenced in some cases by a full stomach which emptied during simulation or adaptation since this could cause large displacements of the stomach and other gastrointestinal OARs. This particularly presents an issue if the levels of stomach content differ considerably between simulation and adaptation. Furthermore, especially large organ movements during adaptation of up to 23 mm could not be detected in all cases. One possible explanation might be that the movement amplitudes of OARs were just considerably larger during adaptation compared to simulation. Different amounts of gas can be found inside stomach and small bowel over the

course of a day (Mostafaei et al. 2018). If simulation and adaptation were performed at different times of the day this might explain the varying motility of these OARs.

Maximum organ movements during simulation, which were too small compared to those detected during adaptation, might be caused by too short simulation times or insufficient number of simulation images. Since the focus of patient selection for this retrospective analysis was on the position of OARs relative to the PTV, the duration of the simulation session and number of simulation images varied greatly between patients. Therefore, further studies are necessary to verify these results and to better identify possible causes for a lack of agreement between organ movement during simulation and adaptation.

Patient-specific margins for organs at risk could be applied in adaptive treatments to achieve more robust results and reduce the effect of intrafractional changes. The proposed method for establishing range of organ movement could be used for this purpose. As it is margin-based, isotropic margins could be derived directly from the RoM values determined from simulation images. A majority of organ movements during adaptation would be covered by this margin, if the aforementioned requirements for a reliable determination of $RoM_{Sim,\,max}$ were met. Isotropic margins could be advantageous because they are a straightforward method to create planning organ at risk volumes and therefore can be easily integrated into everyday clinical practice. However, isotropic margins might also lead to heavily impaired target volume coverage in case OARs are close to the PTV and large margins are necessary to compensate for organ movement. There are also some areas inside the PRV structure which might be rarely or even never occupied by the OAR. This is supported by the fact that the extent of organ movement in some fractions is distinctly higher compared to other fractions. By using a single isotropic margin to cover the maximum organ movement in all adapted fractions, the organ movement would be overestimated in a significant proportion of the adapted fractions, which in turn would lead to an unnecessary reduction of target volume coverage.

Previously, some studies explored the possibility of more complex PRV structures with either patient-specific margins based on coverage probability (Hysing et al. 2006; Hysing et al. 2011) or organ-specific margins based on statistical models (Nakamura et al. 2021). These approaches could be used to create more complex PRV structures with data from simulation MR images. These PRVs could be able to compensate for intrafractional organ movement in an equal way as isotropic margins, while they encompass a smaller volume and therefore have a smaller impact on target volume coverage. The use of simulation MR images would further offer the

advantage of no additional radiation dose being applied and as a consequence the number of images that could be acquired to determine the PRV would not be limited.

In summary, results from this analysis suggest that it is possible to determine maximum OAR movement before the first treatment for most patients. The maximum organ movement detected in simulation MR images could be directly used to define isotropic margins for OARs. Further studies need to show if simulation images could also be used to create more complex and smaller PRV volumes compared to those created with isotropic margins. By applying these patient-specific PRVs in adaptive treatments, more robust results could be obtained. However, the analyzed data was gained from adaptation sessions that took up two hours. This raises the question whether the impact of intrafractional changes might be significantly less pronounced for shorter adaptation times, which will be further discussed in the following chapter.

4.3 Hypothesis – "Shorter adaptation times do not necessarily lead to more robust results"

As already mentioned in the introduction, the possibility to reduce adaptation times in order to mitigate the effect of intrafractional organ at risk movement and receive a more robust adaptation result has previously been discussed (Benitez et al. 2024; Chin et al. 2020; Guckenberger et al. 2024; Sritharan and Tree 2022). However, the previously presented results indicate that it might not be sufficient to just achieve shorter adaptation times.

No correlation was found between the duration of adaptation and intrafractional dose changes. For the evaluated adaptation times between 36 and 110 minutes, a longer duration did not lead to higher differences between adapted and pre-irradiation dose. Additionally, the extent of organ movement for time spans below 36 minutes was analyzed using simulation MR images. Evaluated simulation sessions ranged between 1.5 and 29 minutes and even for short durations below six minutes organ movement up of to 7.5 mm was detected. This extent of OAR movement was associated with dose changes of more than 20% of the respective tolerance dose, which was shown in a correlation analysis between range of OAR movement during adaptation and intrafractional dose changes.

Gastrointestinal motion velocities of up to 2 mm/min were found by Liu et al., supporting the assumption that large positional variations might occur in a short time span (Liu et al. 2021). Furthermore, a planning study of SBRT treatments of pancreatic cancer showed that short term displacements of gastrointestinal OARs within a median timeframe of 12 minutes could lead to a significant increase in organ dose and subsequent tolerance dose violation (Uchinami et al. 2023). However, treatment times of adaptive MRgRT less than 12 minutes appear to be unachievable at the moment. Evaluated adaptation times were consistent with previously published data for abdominal malignancies. Henke et al. reported median adaptation times of 79.0 minutes with a range from 36 to 160 minutes (Henke et al. 2018a). Similar results were found by Tyagi et al. in treatments of pancreatic cancer with a median adaptation time of 75.5 minutes (49 – 132 minutes) (Tyagi et al. 2021), for various abdominal lesions by Garcia Schüler et al. with a mean of 61 minutes (36 – 110 minutes)(Garcia Schüler et al. 2021) and for adrenal gland metastases by Michalet et al. with a median of 78 minutes (Michalet et al. 2022a). Slightly higher median or mean treatment times determined in these studies were probably due

to the inclusion of patient positioning and treatment delivery in total treatment times, which were not part of the analyzed adaptation times between MRI_A and MRI_{pI}.

Even though current treatment times in MR-guided radiotherapy of abdominal lesions are quite long, shorter durations can probably be achieved. The patients evaluated in this analysis were treated up to one year after the introduction of adaptive radiotherapy at Heidelberg University Hospital. During this time, the personnel working at the MR-linac was able to gain more experience, especially regarding OAR recontouring and plan reoptimization, which in turn also led to less time spent for each step. Additionally, changes in the planning technique were introduced since then, leading to more robust plans for reoptimization. As a result, less time-consuming adjustments to the plan are necessary for a majority of plans. Since an upgrade of the treatment delivery software, it is also possible to perform contouring during the adaptation workflow in parallel on up to three workstations, which has shortened the duration of this part of the workflow. In the future the inclusion of automation in the adaptive workflow, e.g. automatic contouring of OARs, might further reduce on-table times of patients.

However, large positional changes in gastrointestinal organs close to the PTV leading to higher organ doses might occur, even if treatment times could be reduced well below ten minutes. Near real-time re-planning would be necessary to mitigate adverse effects of intrafractional organ movement. Even though the possibility of real-time re-planning has been previously explored (Kontaxis et al. 2015; Kontaxis et al. 2017), use in clinical routine is still not possible mainly due to limitations of the necessary computational power (Fast et al. 2024). In conclusion, it is not sufficient to just reduce adaptation times in order to achieve more robust adaptation results. Intrafractional changes still need to be considered even if adaptation times will be significantly reduced in the future.

4.4 Limitations of this analysis

There are some limitations to the presented results. One limitation of the dosimetric analysis is the lack of information on the benefit of adaptation and the impact of intrafractional changes on target volumes. OAR tolerance dose was met in all dose distribution variants in more than half of the analyzed cases and therefore the primary intention of adapting the base plan was either increasing target volume coverage or reducing hotspots. Since target volumes were not evaluated, no conclusion can be drawn whether target volumes did indeed benefit from plan adaptation or if dosimetric benefits for target volumes were also negated by intrafractional changes.

Furthermore, separate statistical analysis of organs at risk to determine possible differences between organ types was not possible since the number of patients included was too small. Retrospective manual recontouring of OARs and generation of dose distribution variants was very time consuming and as result the number of patients was limited to twenty. A larger patient collective is needed in a further analysis in order to evaluate differences between gastrointestinal OARs concerning intrafractional changes and subsequent effects on dose.

For the evaluation of organ range of movement, the mean distance of the organ tolerance isodose from the PTV was used to determine the relevant area for analysis. However, the mean distance of the tolerance dose is only known after treatment planning has been finalized. If RoM values are needed before treatment planning in order to create PRVs, a different parameter might be necessary to define the area in which organ movement is evaluated. Another possible solution could be the use of organ-specific mean distances of the tolerance isodose calculated from multiple patients with the same relevant OAR and comparable treated lesions.

Furthermore, all evaluations were performed with data from MR images acquired at one specific point in time. It is to be expected that displacements of gastrointestinal OARs might happen any time during treatment and result in changes in OAR position relative to the PTV and subsequent changes in dose. Although only a snapshot of the adaptive treatment is considered in the presented evaluations, the results indicate that intrafractional changes might in fact have a relevant influence on the adaptation result.

4.5 Conclusion

The statement "You see what you treat." is closely associated with MR-guided radiotherapy. The excellent soft tissue contrast of MR imaging allows for exact localization of tumors and surrounding organs for each treatment fraction and plans can be adjusted accordingly. However, the MR image used for plan adaptation is only a snapshot of the patient's anatomy at the time of image acquisition. This study has shown that the position of organs at risk relative to the target volume can change considerably during adaptation, which was one of the main reasons the benefit of adaptation was mitigated or even completely negated in some cases, at least concerning OAR dose. In addition, intrafractional organ movement will possibly still remain relevant even if adaptation times can be shortened in the foreseeable future through improved automation in the adaptive workflow.

The use of patient-specific PRVs generated with the help of simulation images could reduce the effects of intrafractional changes and lead to more robust adaptation results, but application of isotropic margins to create these PRVs can lead to heavily impaired PTV coverage. At the same time, most methods for generating non-isotropic margins are quite complex and therefore might not be easily implemented in routine clinical practice. Even if the PRV concepts are not implemented in clinical routine in the near future, the proposed method for determining maximum range of organ movement based on simulation MR images might still be useful. It could be applied in the clinical workflow to evaluate in which cases a special focus should be placed on OAR position relative to the PTV when assessing pre-irradiation MR. This step could be facilitated further by manufacturers integrated the option to acquire a second MR image into their adaptive workflow because it would require considerably less time compared to the current workflow.

Furthermore, the dosimetric impact of intrafractional organ movement could be assessed more easily if a fast estimation of OAR dose on pre-irradiation MR images was possible. This would require integration of accurate auto-contouring of OARs in combination with fast dose prediction in the treatment software. Although a lot of research has been conducted on auto-contouring based on MR images and it could be of great advantage during adaptation, it has not yet been integrated into the ViewRay MRIdian adaptation workflow.

In addition, tracking or even beam gating of relevant OARs during irradiation using cine imaging could be considered in the future. So far, beam gating is mainly focused on target volumes and it first needs to be evaluated whether beam gating of OARs is feasible in clinical practice. Furthermore, cine imaging is currently limited to a few 2D slices. A future implementation of 2D cine imaging with more slices than currently available or even the introduction of 3D cine imaging on MR-linacs could further facilitate beam gating of organ at risk structures.

Although only lower grade toxicities of organs at risk are currently reported in adaptive MR-guided radiotherapy, intrafractional organ movement and subsequent higher OAR doses might need to be considered in the future, particularly for re-irradiation scenarios and dose escalation trials. Dose accumulation of treatment fractions could give a better approximation of the dose which was actually applied to OARs in adaptive treatments. However, dose accumulation currently has to be carried out manually, which prevents it from being performed routinely. The same applies to the creation of pre-irradiation dose distributions. Since they are not automatically generated by the treatment system and their creation is currently time-consuming, pre-irradiation dose is usually not reviewed retrospectively. As with previously described functionalities, routine review of accumulated dose as well as pre-irradiation OAR dose could be achieved by integrating these features into the manufacturer's software.

Although prospective tools will presumably make it easier to recognize intrafractional changes and react accordingly, it is uncertain how long it will take to introduce them into the clinical routine. Therefore, it is essential that everyone involved in MR-guided radiotherapy treatments is aware of the fact that what can be seen on one MR image acquired at the start of a treatment session does not necessarily correspond to what is actually being treated. Even though adaptation can be used to react to changes between treatment fractions, the acquired MR images remain a snapshot and changes can occur at any time during treatment, thereby mitigating patient benefit of adaptive MR-guided radiotherapy.

5 SUMMARY

Magnetic resonance (MR)-guided radiotherapy enables daily adaptation of a patient's treatment plan to the current patient anatomy. Previous reports have already shown the resulting advantages, especially good sparing of organs at risk while simultaneously achieving optimal target volume coverage. However, patient geometry can change during the adaptation process, which takes significantly longer than conventional radiotherapy treatments. So far, there is limited research on the effects of these intrafractional changes. In particular, gastrointestinal organs at risk might exhibit large shifts and deformations, which could also have a negative impact on the benefits gained by adaptive radiotherapy. In order to evaluate the impact of intrafractional organ movement and allow for patient-specific compensation, it is necessary to determine the extent of organ movement before the first adaptive treatment. Simulation MR-images acquired for treatment planning could offer this possibility, as they do not require additional dose to the patient and therefore a large number can be acquired to determine organ movement. However, adaptation currently takes a very long time with reported adaptation times of one hour or more. This raises the question of whether a more robust result could be achieved with shorter adaptation times. As a result, the following hypotheses will be investigated:

1) "In some cases, adaptation has no benefit"
2) "More robust adaptive treatments can be obtained by predicting the extent of intrafractional organ movement before the first treatment"
3) "Shorter adaptation times do not necessarily lead to more robust results"

Patients who received adaptive MR-guided radiotherapy for the treatment of abdominal lesions were retrospectively analyzed. The main focus of this study was on lesions located in close proximity to organs at risk. Dose differences in organs at risk caused by adaptation as well as by intrafractional changes were determined. Furthermore, the range of organ movement during simulation and adaptation was determined for each patient and agreement between both values was examined. In addition, the duration of adaptation and simulation sessions was determined in order to establish a possible correlation between the extent of organ movements and the magnitude of dose differences.

The evaluation of dose differences shows that the number of violations of organ at risk tolerance dose could be significantly reduced by adaptation. However, an increase in organ dose was also observed in the majority of patients as a result of adaptation, while respective tolerance dose

was still met. Possible causes for this increase are either a lack of optimization objective for organs at risk with some distance to the PTV or the possibility to increase organ dose in order to optimize target volume coverage while still not violating tolerance doses. Additionally, the number of tolerance dose violations increased again as a result of intrafractional changes, and it was even higher than it would have been without plan adaptation. Using simulation MR-images, the extent of risk organ movement can already be determined before the first treatment, though, which opens up the possibility of compensating for intrafractional changes. With the method presented in this study, there was an agreement between the range of organ at risk movement during adaptation and simulation in over 75% of analyzed cases. Acquisition of multiple simulation images and a longer simulation duration led to better overall agreement. In addition, there was no correlation between adaptation time and the magnitude of dose change for the adaptation times examined in this study. This signifies that a longer duration does not lead to a greater dose difference. Furthermore, evaluation of simulation images showed large organ at risk movement in a short time span of only five minutes and no correlation between the extent of organ movement and the duration of simulation sessions could be found.

Overall, these results demonstrate that adaptation has no benefit in some cases, at least when considering the dosimetric advantage for organs at risk. In particular, intrafractional organ movement leads to violations of organ at risk tolerance dose. However, the extent of these organ movements can be determined in advance with the help of the simulation images. As a result, a special focus can be put on those organs at risk with a high mobility and it opens up the possibility to compensate for them. Major changes in the position of gastrointestinal organs at risk can occur within a very short time span. Therefore, it does not appear to be sufficient to simply shorten the adaptation time in order to achieve a more robust adaptation result.

6 ZUSAMMENFASSUNG

Die Magnetresonanz (MR)-gestützte Strahlentherapie ermöglich eine tägliche Adaption des Bestrahlungsplans an die aktuelle Patientengeometrie. Die entstehenden Vorteile, insbesondere eine gute Risikoorganschonung bei gleichzeitig möglichst optimaler Auslastung von Zielvolumina, wurde bereits vielfach belegt. Allerdings kann sich die Patientengeometrie während der Adaption, welche deutlich länger dauert als herkömmliche Strahlentherapie-behandlungen, ändern. Bislang wurden die Auswirkungen dieser intrafraktionellen Änderungen wenig untersucht. Vor allem gastrointestinale Risikoorgane weisen teilweise große Verschiebungen und Deformationen auf, welche sich auch negativ auf den Nutzen der adaptiven Therapie auswirken könnte. Um intrafraktionelle Organbewegungen erkennen und für jeden Patienten individuell kompensieren zu können, ist es notwendig, diese bereits vor der ersten adaptiven Behandlung zu erkennen. Für die Bestrahlungsplanung aufgenommenen MR-Simulationsbilder könnten die Möglichkeit dazu bieten, da sie ohne zusätzliche Dosis auskommen und somit eine große Anzahl aufgenommen werden kann, um die Organbewegung zu bestimmen. Die Adaption dauert aktuell jedoch sehr lange und es wird häufig eine Dauer von einer Stunde oder mehr berichtet. Dies wirft die Frage auf, ob durch kürzere Adaptionszeiten ein robusteres Ergebnis erzielt werden kann. Daraus ergeben sich die folgenden Hypothesen, welche in dieser Studie untersucht werden sollen:

1) „In einigen Fällen hat die Adaption keinen Nutzen“
2) „Robustere adaptive Behandlungen können erzielt werden, indem das Ausmaß von Organbewegungen vor der ersten Behandlung ermittelt wird“
3) „Kürzere Adaptionszeiten führen nicht unbedingt zu robusteren Ergebnissen“

Dazu wurden retrospektiv Patienten untersucht, welche eine adaptive MR-geführte Strahlentherapie zur Behandlung von abdominellen Läsionen erhielten. Der Hauptfokus war dabei auf Läsionen, welche in unmittelbarer Nähe zu Risikoorganen lagen. Es wurden die Dosisunterschiede in Risikoorganen bestimmt, welche sich durch Adaption sowie durch intrafraktionelle Änderungen ergaben. Außerdem wurde das Ausmaß der Organbewegungen bei Simulation und Adaption für jeden Patienten bestimmt und auf eine mögliche Übereinstimmung untersucht. Zudem wurde die Dauer von Adaption und Simulation ermittelt, um einen möglichen Zusammenhang zum Ausmaß der Organbewegungen und der Höhe von Dosisunterschieden festzustellen.

Die Untersuchung der Dosisunterschiede zeigt, dass die Anzahl der Fraktionen, bei denen die Toleranzdosis der Risikoorgane nicht eingehalten werden konnte, durch Adaption deutlich reduziert werden konnte. Allerdings konnte bei einem Großteil der Patienten auch ein Anstieg der Organdosis unterhalb der Toleranzdosis durch die Adaption beobachtet werden. Mögliche Ursachen dafür sind entweder eine fehlende Optimierungsvorgabe oder die Möglichkeit eine höhere Risikoorgandosis unterhalb der Toleranzdosis zuzulassen, um das Zielvolumen optimal auszulasten. Durch intrafraktionelle Änderungen stieg die Anzahl der nichteingehaltenen Risikoorganvorgaben wieder an, sodass kurz vor Bestrahlung mehr Vorgaben nicht eingehalten wurden, als wenn der Grundplan bestrahlt worden wäre. Zudem konnte insgesamt ein statistisch signifikanter Anstieg der Risikoorgandosis durch intrafraktionelle Änderungen festgestellt werden. Allerdings kann das Ausmaß der Risikoorganbewegung bereits vor der ersten Behandlung mit Hilfe von MR-Simulationsbildern bestimmt werden, wodurch die Möglichkeit eröffnet wird, diese zu kompensieren. Mit der in dieser Studie vorgestellten Methode, liegt die Übereinstimmung des Ausmaßes der Risikoorganbewegung bei Adaption und Simulation bei über 75%. Dabei führen die Aufnahme mehrerer Simulationsbilder und eine längere Simulationsdauer insgesamt zu einer besseren Übereinstimmung. Darüber hinaus liegt für die untersuchten Adaptionszeiten keine Korrelation zwischen Adaptionsdauer und Höhe der Dosisänderung vor, was bedeutet, dass eine längere Dauer nicht zu einer größeren Änderung führt. Zudem zeigt die Analyse der Simulationsbilder, dass große Risikoorganbewegungen bereits innerhalb von fünf Minuten auftreten können. Auch für die kürzeren Zeiten der Simulationssitzungen konnte keine Korrelation mit dem Ausmaß der Organbewegung festgestellt werden.

Insgesamt folgt aus diesen Ergebnissen, dass die Adaption in einigen Fällen keinen Nutzen hat, wenn man den dosimetrischen Vorteil in Risikoorganen betrachtet. Insbesondere intrafraktionelle Organbewegungen führen dazu, dass die Toleranzdosis in Risikoorganen überschritten wird. Das Ausmaß dieser Organbewegungen kann jedoch mit Hilfe der Simulationsbilder bereits im Voraus bestimmt werden. Dies bietet die Möglichkeit, bei der Behandlung einen speziellen Fokus auf Risikoorgane mit großer Beweglichkeit zu legen und diese möglicherweise zu kompensieren. Zudem können große Lageveränderungen von gastrointestinalen Risikoorganen bereits innerhalb sehr kurzer Zeit auftreten. Daher erscheint es nicht ausreichend, nur die Adaptionsdauer zu verkürzen, um ein robusteres Adaptionsergebnis zu erhalten.

7 BIBLIOGRAPHY

Acharya, S., Fischer-Valuck, B. W., Kashani, R., Parikh, P., Yang, D., Zhao, T., Green, O., Wooten, O., Li, H. H., Hu, Y., Rodriguez, V., Olsen, L., Robinson, C., Michalski, J., Mutic, S. and Olsen, J. (2016). **Online Magnetic Resonance Image Guided Adaptive Radiation Therapy: First Clinical Applications**. Int J Radiat Oncol Biol Phys *94 (2)*, 394-403, doi: 10.1016/j.ijrobp.2015.10.015.

Alam, S., Veeraraghavan, H., Tringale, K., Amoateng, E., Subashi, E., Wu, A. J., Crane, C. H. and Tyagi, N. (2022). **Inter- and intrafraction motion assessment and accumulated dose quantification of upper gastrointestinal organs during magnetic resonance-guided ablative radiation therapy of pancreas patients**. Phys Imaging Radiat Oncol *21*, 54-61, doi: 10.1016/j.phro.2022.02.007.

Andratschke, N., Willmann, J., Appelt, A. L., Alyamani, N., Balermpas, P., Baumert, B. G., Hurkmans, C., Hoyer, M., Langendijk, J. A., Kaidar-Person, O., van der Linden, Y., Meattini, I., Niyazi, M., Reynaert, N., De Ruysscher, D., Tanadini-Lang, S., Hoskin, P., Poortmans, P. and Nieder, C. (2022). **European Society for Radiotherapy and Oncology and European Organisation for Research and Treatment of Cancer consensus on re-irradiation: definition, reporting, and clinical decision making**. Lancet Oncol *23 (10)*, e469-e478, doi: 10.1016/S1470-2045(22)00447-8.

Bates, D., Mächler, M., Bolker, B. and Walker, S. (2015). **Fitting Linear Mixed-Effects Models Usinglme4**. Journal of Statistical Software *67 (1)*, doi: 10.18637/jss.v067.i01.

Battista, J. J., Rider, W. D. and Van Dyk, J. (1980). **Computed tomography for radiotherapy planning**. Int J Radiat Oncol Biol Phys *6 (1)*, 99-107, doi: 10.1016/0360-3016(80)90211-4.

Benedict, S. H., Yenice, K. M., Followill, D., Galvin, J. M., Hinson, W., Kavanagh, B., Keall, P., Lovelock, M., Meeks, S., Papiez, L., Purdie, T., Sadagopan, R., Schell, M. C., Salter, B., Schlesinger, D. J., Shiu, A. S., Solberg, T., Song, D. Y., Stieber, V., Timmerman, R., Tome, W. A., Verellen, D., Wang, L. and Yin, F. F. (2010). **Stereotactic body radiation therapy: the report of AAPM Task Group 101**. Med Phys *37 (8)*, 4078-4101, doi: 10.1118/1.3438081.

Benitez, C. M., Chuong, M. D., Kunzel, L. A. and Thorwarth, D. (2024). **MRI-Guided Adaptive Radiation Therapy**. Semin Radiat Oncol *34 (1)*, 84-91, doi: 10.1016/j.semradonc.2023.10.013.

Blomgren, H., Lax, I., Naslund, I. and Svanstrom, R. (1995). **Stereotactic high dose fraction radiation therapy of extracranial tumors using an accelerator. Clinical experience of the first thirty-one patients**. Acta Oncol *34 (6)*, 861-870, doi: 10.3109/02841869509127197.

Bohoudi, O., Bruynzeel, A. M. E., Meijerink, M. R., Senan, S., Slotman, B. J., Palacios, M. A. and Lagerwaard, F. J. (2019). **Identification of patients with locally advanced pancreatic cancer benefitting from plan adaptation in MR-guided radiation therapy**. Radiother Oncol *132*, 16-22, doi: 10.1016/j.radonc.2018.11.019.

Bohoudi, O., Bruynzeel, A. M. E., Senan, S., Cuijpers, J. P., Slotman, B. J., Lagerwaard, F. J. and Palacios, M. A. (2017). **Fast and robust online adaptive planning in stereotactic MR-guided adaptive radiation therapy (SMART) for pancreatic cancer**. Radiother Oncol *125 (3)*, 439-444, doi: 10.1016/j.radonc.2017.07.028.

Bordeau, K., Michalet, M., Keskes, A., Valdenaire, S., Debuire, P., Cantaloube, M., Cabaille, M., Portales, F., Draghici, R., Ychou, M., Assenat, E., Mazard, T., Samalin, E., Gauthier, L., Colombo, P. E., Carrere, S., Souche, F. R., Ailleres, N., Fenoglietto, P., Azria, D. and Riou, O. (2022). **Stereotactic MR-Guided Adaptive Radiotherapy for Pancreatic Tumors: Updated Results of the Montpellier Prospective Registry Study**. Cancers (Basel) *15 (1)*, doi: 10.3390/cancers15010007.

Buchele, C., Renkamp, C. K., Regnery, S., Behnisch, R., Rippke, C., Schlüter, F., Hoegen-Saßmannshausen, P., Debus, J., Hörner-Rieber, J., Alber, M. and Klüter, S. (2024). **Intrafraction organ movement in adaptive MR-guided radiotherapy of abdominal lesions – dosimetric impact and how to detect its extent in advance**. Submitted to Radiation Oncology. Revised manuscript currently under review.

Chen, W. C., Baal, J. D., Baal, U., Pai, J., Gottschalk, A., Boreta, L., Braunstein, S. E. and Raleigh, D. R. (2020). **Stereotactic Body Radiation Therapy of Adrenal Metastases: A Pooled Meta-Analysis and Systematic Review of 39 Studies with 1006 Patients**. Int J Radiat Oncol Biol Phys *107 (1)*, 48-61, doi: 10.1016/j.ijrobp.2020.01.017.

Chin, S., Eccles, C. L., McWilliam, A., Chuter, R., Walker, E., Whitehurst, P., Berresford, J., Van Herk, M., Hoskin, P. J. and Choudhury, A. (2020). **Magnetic resonance-guided radiation therapy: A review**. J Med Imaging Radiat Oncol *64 (1)*, 163-177, doi: 10.1111/1754-9485.12968.

Corradini, S., Alongi, F., Andratschke, N., Belka, C., Boldrini, L., Cellini, F., Debus, J., Guckenberger, M., Hörner-Rieber, J., Lagerwaard, F. J., Mazzola, R., Palacios, M. A., Philippens, M. E. P., Raaijmakers, C. P. J., Terhaard, C. H. J., Valentini, V. and Niyazi, M. (2019). **MR-guidance in clinical reality: current treatment challenges and future perspectives**. Radiat Oncol *14 (1)*, 92, doi: 10.1186/s13014-019-1308-y.

Cusumano, D., Dhont, J., Boldrini, L., Chiloiro, G., Teodoli, S., Massaccesi, M., Fionda, B., Cellini, F., Azario, L., Vandemeulebroucke, J., De Spirito, M., Valentini, V. and Verellen, D. (2018). **Predicting tumour motion during the whole radiotherapy treatment: a systematic approach for thoracic and abdominal lesions based on real time MR**. Radiother Oncol *129 (3)*, 456-462, doi: 10.1016/j.radonc.2018.07.025.

Daly, M. E. (2022). **Inoperable Early-Stage Non-Small-Cell Lung Cancer: Stereotactic Ablative Radiotherapy and Rationale for Systemic Therapy**. J Clin Oncol *40 (6)*, 539-545, doi: 10.1200/JCO.21.01611.

Dawson, L. A. and Menard, C. (2010). **Imaging in radiation oncology: a perspective**. Oncologist *15 (4)*, 338-349, doi: 10.1634/theoncologist.2009-S106.

Dobbs, H. J., Parker, R. P., Hodson, N. J., Hobday, P. and Husband, J. E. (1983). **The use of CT in radiotherapy treatment planning**. Radiother Oncol *1 (2)*, 133-141, doi: 10.1016/s0167-8140(83)80016-4.

Eijkelenkamp, H., Grimbergen, G., Daamen, L. A., Heerkens, H. D., van de Ven, S., Mook, S., Meijer, G. J., Molenaar, I. Q., van Santvoort, H. C., Paulson, E., Erickson, B. A., Verkooijen, H. M., Hall, W. A. and Intven, M. P. W. (2023). **Clinical outcomes after online adaptive MR-guided stereotactic body radiotherapy for pancreatic tumors on a 1.5 T MR-linac**. Front Oncol *13*, 1040673, doi: 10.3389/fonc.2023.1040673.

Fagerland, M. W. (2023). **contingencytables: Statistical Analysis of Contingency Tables**. URL: https://CRAN.R-project.org/package=contingencytables [Accessed: 16.11.2023].

Fagerland, M. W., Lydersen, S. and Laake, P. (2013). **The McNemar test for binary matched-pairs data: mid-p and asymptotic are better than exact conditional**. BMC Med Res Methodol *13*, 91, doi: 10.1186/1471-2288-13-91.

Fast, M. F., Cao, M., Parikh, P. and Sonke, J. J. (2024). **Intrafraction Motion Management With MR-Guided Radiation Therapy**. Semin Radiat Oncol *34 (1)*, 92-106, doi: 10.1016/j.semradonc.2023.10.008.

Garcia Schüler, H. I., Pavic, M., Mayinger, M., Weitkamp, N., Chamberlain, M., Reiner, C., Linsenmeier, C., Balermpas, P., Krayenbuhl, J., Guckenberger, M., Baumgartl, M., Wilke, L., Tanadini-Lang, S. and Andratschke, N. (2021). **Operating procedures, risk management and challenges during implementation of adaptive and non-adaptive MR-guided radiotherapy: 1-year single-center experience**. Radiat Oncol *16 (1)*, 217, doi: 10.1186/s13014-021-01945-9.

Guckenberger, M., Andratschke, N., Chung, C., Fuller, D., Tanadini-Lang, S. and Jaffray, D. A. (2024). **The Future of MR-Guided Radiation Therapy**. Semin Radiat Oncol *34 (1)*, 135-144, doi: 10.1016/j.semradonc.2023.10.015.

Guckenberger, M., Baus, W. W., Blanck, O., Combs, S. E., Debus, J., Engenhart-Cabillic, R., Gauer, T., Grosu, A. L., Schmitt, D., Tanadini-Lang, S. and Moustakis, C. (2020). **Definition and quality requirements for stereotactic radiotherapy: consensus statement from the DEGRO/DGMP Working Group Stereotactic Radiotherapy and Radiosurgery**. Strahlenther Onkol *196 (5)*, 417-420, doi: 10.1007/s00066-020-01603-1.

Guckenberger, M., Meyer, J., Wilbert, J., Baier, K., Mueller, G., Wulf, J. and Flentje, M. (2006). **Cone-beam CT based image-guidance for extracranial stereotactic radiotherapy of intrapulmonary tumors**. Acta Oncol *45 (7)*, 897-906, doi: 10.1080/02841860600904839.

Guckenberger, M., Sweeney, R. A., Wilbert, J., Krieger, T., Richter, A., Baier, K., Mueller, G., Sauer, O. and Flentje, M. (2008). **Image-guided radiotherapy for liver cancer using respiratory-correlated computed tomography and cone-beam computed tomography**. Int J Radiat Oncol Biol Phys *71 (1)*, 297-304, doi: 10.1016/j.ijrobp.2008.01.005.

Guckenberger, M., Wulf, J., Mueller, G., Krieger, T., Baier, K., Gabor, M., Richter, A., Wilbert, J. and Flentje, M. (2009). **Dose-response relationship for image-guided stereotactic body radiotherapy of pulmonary tumors: relevance of 4D dose calculation**. Int J Radiat Oncol Biol Phys *74 (1)*, 47-54, doi: 10.1016/j.ijrobp.2008.06.1939.

Hanna, G. G., Murray, L., Patel, R., Jain, S., Aitken, K. L., Franks, K. N., van As, N., Tree, A., Hatfield, P., Harrow, S., McDonald, F., Ahmed, M., Saran, F. H., Webster, G. J., Khoo, V., Landau, D., Eaton, D. J. and Hawkins, M. A. (2018). **UK Consensus on Normal Tissue Dose Constraints for Stereotactic Radiotherapy**. Clin Oncol (R Coll Radiol) *30 (1)*, 5-14, doi: 10.1016/j.clon.2017.09.007.

Haseltine, J. M., Rimner, A., Gelblum, D. Y., Modh, A., Rosenzweig, K. E., Jackson, A., Yorke, E. D. and Wu, A. J. (2016). **Fatal complications after stereotactic body radiation therapy for central lung tumors abutting the proximal bronchial tree**. Pract Radiat Oncol *6 (2)*, e27-33, doi: 10.1016/j.prro.2015.09.012.

Henke, L., Kashani, R., Robinson, C., Curcuru, A., DeWees, T., Bradley, J., Green, O., Michalski, J., Mutic, S., Parikh, P. and Olsen, J. (2018a). **Phase I trial of stereotactic MR-guided online adaptive radiation therapy (SMART) for the treatment of oligometastatic or unresectable primary malignancies of the abdomen**. Radiother Oncol *126 (3)*, 519-526, doi: 10.1016/j.radonc.2017.11.032.

Henke, L. E., Green, O. L., Curcuru, A., Lu, Y., Mutic, S., Parikh, P. J. and Kashani, R. (2018b). **Magnitude and Dosimetric Impact of Inter- and Intra-Fraction Anatomic Variability During MRI-Guided Online Adaptive Radiation Therapy (MRgART) to the Abdomen**. International Journal of Radiation Oncology Biology Physics *102 (3)*, S129-S130, doi: 10.1016/j.ijrobp.2018.06.321.

Hoegen, P., Katsigiannopulos, E., Buchele, C., Regnery, S., Weykamp, F., Sandrini, E., Ristau, J., Liermann, J., Meixner, E., Forster, T., Renkamp, C. K., Schluter, F., Rippke, C., Debus, J., Klüter, S. and Hörner-Rieber, J. (2023). **Stereotactic magnetic resonance-guided online adaptive radiotherapy of adrenal metastases combines high ablative doses with optimized sparing of organs at risk**. Clin Transl Radiat Oncol *39*, 100567, doi: 10.1016/j.ctro.2022.100567.

Hof, H., Herfarth, K. K., Munter, M., Hoess, A., Motsch, J., Wannenmacher, M. and Debus, J. J. (2003). **Stereotactic single-dose radiotherapy of stage I non-small-cell lung cancer (NSCLC)**. Int J Radiat Oncol Biol Phys *56 (2)*, 335-341, doi: 10.1016/s0360-3016(02)04504-2.

Holyoake, D. L. P., Robinson, M., Silva, M., Grose, D., McIntosh, D., Sebag-Montefiore, D., Radhakrishna, G., Mukherjee, S. and Hawkins, M. A. (2021). **SPARC, a phase-I trial of pre-operative, margin intensified, stereotactic body radiation therapy for pancreatic cancer**. Radiother Oncol *155*, 278-284, doi: 10.1016/j.radonc.2020.11.007.

Hounsfield, G. N. (1973). **Computerized transverse axial scanning (tomography). 1. Description of system**. Br J Radiol *46 (552)*, 1016-1022, doi: 10.1259/0007-1285-46-552-1016.

Hysing, L. B., Kvinnsland, Y., Lord, H. and Muren, L. P. (2006). **Planning organ at risk volume margins for organ motion of the intestine**. Radiother Oncol *80 (3)*, 349-354, doi: 10.1016/j.radonc.2006.07.039.

Hysing, L. B., Sohn, M., Muren, L. P. and Alber, M. (2011). **A coverage probability based method to estimate patient-specific small bowel planning volumes for use in radiotherapy**. Radiother Oncol *100 (3)*, 407-411, doi: 10.1016/j.radonc.2011.08.037.

Jaffray, D. A., Drake, D. G., Moreau, M., Martinez, A. A. and Wong, J. W. (1999). **A radiographic and tomographic imaging system integrated into a medical linear accelerator for localization of bone and soft-tissue targets**. Int J Radiat Oncol Biol Phys *45 (3)*, 773-789, doi: 10.1016/s0360-3016(99)00118-2.

Jelden, G. L., Chernak, E. S., Rodriguez-Antunez, A., Haaga, J. R., Lavik, P. S. and Dhaliwal, R. S. (1976). **Further progress in CT scanning and computerized radiation therapy treatment planning**. AJR Am J Roentgenol *127 (1)*, 179-185, doi: 10.2214/ajr.127.1.179.

Kashani, R. and Olsen, J. R. (2018). **Magnetic Resonance Imaging for Target Delineation and Daily Treatment Modification**. Semin Radiat Oncol *28 (3)*, 178-184, doi: 10.1016/j.semradonc.2018.02.002.

Katz, A. W., Carey-Sampson, M., Muhs, A. G., Milano, M. T., Schell, M. C. and Okunieff, P. (2007). **Hypofractionated stereotactic body radiation therapy (SBRT) for limited hepatic metastases**. Int J Radiat Oncol Biol Phys *67 (3)*, 793-798, doi: 10.1016/j.ijrobp.2006.10.025.

Kavanagh, B. D., Pan, C. C., Dawson, L. A., Das, S. K., Li, X. A., Ten Haken, R. K. and Miften, M. (2010). **Radiation dose-volume effects in the stomach and small bowel**. Int J Radiat Oncol Biol Phys *76 (3 Suppl)*, S101-107, doi: 10.1016/j.ijrobp.2009.05.071.

Kawrakow, I. (2001). **VMC++, Electron and Photon Monte Carlo Calculations Optimized for Radiation Treatment Planning**. Paper presented at: Advanced Monte Carlo for Radiation Physics, Particle Transport Simulation and Applications (Berlin, Heidelberg: Springer Berlin Heidelberg).

Kawrakow, I. and Fippel, M. (2000). **Investigation of variance reduction techniques for Monte Carlo photon dose calculation using XVMC**. Phys Med Biol *45 (8)*, 2163-2183, doi: 10.1088/0031-9155/45/8/308.

Kirkbride, P. and Cooper, T. (2011). **Stereotactic body radiotherapy. Guidelines for commissioners, providers and clinicians: a national report**. Clin Oncol (R Coll Radiol) *23 (3)*, 163-164, doi: 10.1016/j.clon.2011.01.155.

Klüter, S. (2019). **Technical design and concept of a 0.35 T MR-Linac**. Clin Transl Radiat Oncol *18*, 98-101, doi: 10.1016/j.ctro.2019.04.007.

Kok, E. N. D., Jansen, E. P. M., Heeres, B. C., Kok, N. F. M., Janssen, T., van Werkhoven, E., Sanders, F. R. K., Ruers, T. J. M., Nowee, M. E. and Kuhlmann, K. F. D. (2020). **High versus low dose Stereotactic Body Radiation Therapy for hepatic metastases**. Clin Transl Radiat Oncol *20*, 45-50, doi: 10.1016/j.ctro.2019.11.004.

Kontaxis, C., Bol, G. H., Lagendijk, J. J. and Raaymakers, B. W. (2015). **A new methodology for inter- and intrafraction plan adaptation for the MR-linac**. Phys Med Biol *60 (19)*, 7485-7497, doi: 10.1088/0031-9155/60/19/7485.

Kontaxis, C., Bol, G. H., Stemkens, B., Glitzner, M., Prins, F. M., Kerkmeijer, L. G. W., Lagendijk, J. J. W. and Raaymakers, B. W. (2017). **Towards fast online intrafraction replanning for free-breathing stereotactic body radiation therapy with the MR-linac**. Phys Med Biol *62 (18)*, 7233-7248, doi: 10.1088/1361-6560/aa82ae.

Lagendijk, J. J. W. and Bakker, C. J. G. (2000). **MRI guided radiotherapy: a MRI based linear accelerator**. Radiotherapy and Oncology *56 (S1)*, S60-S61.

Landberg, T., Chavaudra, J., Dobbs, J., Gerard, J.-P., Hanks, G., Horiot, J.-C., Johansson, K.-A., Möller, T., Purdy, J., Suntharalingam, N. and Svensson, H. (1999). **2. Volumes**. Reports of the International Commission on Radiation Units and Measurements. ICRU Report 62: Prescribing, Recording and Reporting Photon Beam Therapy (Supplement to ICRU Report 50) *os-32 (1)*, 3-20, doi: 10.1093/jicru_os32.1.3.

Lax, I., Blomgren, H., Naslund, I. and Svanstrom, R. (1994). **Stereotactic radiotherapy of malignancies in the abdomen. Methodological aspects**. Acta Oncol *33 (6)*, 677-683, doi: 10.3109/02841869409121782.

Leksell, L. (1951). **The stereotaxic method and radiosurgery of the brain**. Acta Chir Scand *102 (4)*, 316-319.

Lindberg, K., Grozman, V., Karlsson, K., Lindberg, S., Lax, I., Wersall, P., Persson, G. F., Josipovic, M., Khalil, A. A., Moeller, D. S., Nyman, J., Drugge, N., Bergstrom, P., Olofsson, J., Rogg, L. V., Ramberg, C., Kristiansen, C., Jeppesen, S. S., Nielsen, T. B., Loden, B., Rosenbrand, H. O., Engelholm, S., Haraldsson, A., Billiet, C. and Lewensohn, R. (2021). **The HILUS-Trial-a Prospective Nordic Multicenter Phase 2 Study of Ultracentral Lung Tumors Treated With Stereotactic Body Radiotherapy**. J Thorac Oncol *16 (7)*, 1200-1210, doi: 10.1016/j.jtho.2021.03.019.

Liu, L., Johansson, A., Cao, Y., Kashani, R., Lawrence, T. S. and Balter, J. M. (2021). **Modeling intra-fractional abdominal configuration changes using breathing motion-corrected radial MRI**. Phys Med Biol *66 (8)*, doi: 10.1088/1361-6560/abef42.

Lo, S. S., Sahgal, A., Chang, E. L., Mayr, N. A., Teh, B. S., Huang, Z., Schefter, T. E., Yao, M., Machtay, M., Slotman, B. J. and Timmerman, R. D. (2013). **Serious complications associated with stereotactic ablative radiotherapy and strategies to mitigate the risk**. Clin Oncol (R Coll Radiol) *25 (6)*, 378-387, doi: 10.1016/j.clon.2013.01.003.

Mayinger, M., Ludwig, R., Christ, S. M., Dal Bello, R., Ryu, A., Weitkamp, N., Pavic, M., Garcia Schüler, H., Wilke, L., Guckenberger, M., Unkelbach, J., Tanadini-Lang, S. and Andratschke, N. (2021). **Benefit of replanning in MR-guided online adaptive radiation therapy in the treatment of liver metastasis**. Radiat Oncol *16 (1)*, 84, doi: 10.1186/s13014-021-01813-6.

McDonald, B. A., Zachiu, C., Christodouleas, J., Naser, M. A., Ruschin, M., Sonke, J. J., Thorwarth, D., Letourneau, D., Tyagi, N., Tadic, T., Yang, J., Li, X. A., Bernchou, U., Hyer, D. E., Snyder, J. E., Bubula-Rehm, E., Fuller, C. D. and Brock, K. K. (2022). **Dose accumulation for MR-guided adaptive radiotherapy: From practical considerations to state-of-the-art clinical implementation**. Front Oncol *12*, 1086258, doi: 10.3389/fonc.2022.1086258.

Michalet, M., Bettaieb, O., Khalfi, S., Ghorbel, A., Valdenaire, S., Debuire, P., Ailleres, N., Draghici, R., De Meric De Bellefon, M., Charissoux, M., Boisselier, P., Demontoy, S., Marguerit, A., Cabaille, M., Cantaloube, M., Keskes, A., Bouhafa, T., Farcy-Jacquet, M. P., Fenoglietto, P., Azria, D. and Riou, O. (2022a). **Stereotactic MR-Guided Radiotherapy for Adrenal Gland Metastases: First Clinical Results**. J Clin Med *12 (1)*, doi: 10.3390/jcm12010291.

Michalet, M., Bordeau, K., Cantaloube, M., Valdenaire, S., Debuire, P., Simeon, S., Portales, F., Draghici, R., Ychou, M., Assenat, E., Dupuy, M., Gourgou, S., Colombo, P. E., Carrere, S., Souche, F. R., Ailleres, N., Fenoglietto, P., Azria, D. and Riou, O. (2022b). **Stereotactic MR-Guided Radiotherapy for Pancreatic Tumors: Dosimetric Benefit of Adaptation and First Clinical Results in a Prospective Registry Study**. Front Oncol *12*, 842402, doi: 10.3389/fonc.2022.842402.

Michel, R., Francoise, I., Laure, P., Anouchka, M., Guillaume, P. and Sylvain, K. (2017). **Dose to organ at risk and dose prescription in liver SBRT**. Rep Pract Oncol Radiother *22 (2)*, 96-102, doi: 10.1016/j.rpor.2017.03.001.

Miften, M., Vinogradskiy, Y., Moiseenko, V., Grimm, J., Yorke, E., Jackson, A., Tome, W. A., Ten Haken, R. K., Ohri, N., Mendez Romero, A., Goodman, K. A., Marks, L. B., Kavanagh, B. and Dawson, L. A. (2021). **Radiation Dose-Volume Effects for Liver SBRT**. Int J Radiat Oncol Biol Phys *110 (1)*, 196-205, doi: 10.1016/j.ijrobp.2017.12.290.

Mostafaei, F., Tai, A., Omari, E., Song, Y., Christian, J., Paulson, E., Hall, W., Erickson, B. and Li, X. A. (2018). **Variations of MRI-assessed peristaltic motions during radiation therapy**. PLoS One *13 (10)*, e0205917, doi: 10.1371/journal.pone.0205917.

Nakamura, M., Nakao, M., Mukumoto, N., Ashida, R., Hirashima, H., Yoshimura, M. and Mizowaki, T. (2021). **Statistical shape model-based planning organ-at-risk volume: application to pancreatic cancer patients**. Phys Med Biol *66 (1)*, 014001, doi: 10.1088/1361-6560/abcd1b.

Nieder, C., Andratschke, N. H. and Grosu, A. L. (2013). **Increasing frequency of reirradiation studies in radiation oncology: systematic review of highly cited articles**. Am J Cancer Res *3 (2)*, 152-158.

Nierer, L., Eze, C., da Silva Mendes, V., Braun, J., Thum, P., von Bestenbostel, R., Kurz, C., Landry, G., Reiner, M., Niyazi, M., Belka, C. and Corradini, S. (2022). **Dosimetric benefit of MR-guided online adaptive radiotherapy in different tumor entities: liver, lung, abdominal lymph nodes, pancreas and prostate**. Radiat Oncol *17 (1)*, 53, doi: 10.1186/s13014-022-02021-6.

Ohri, N., Tome, W. A., Mendez Romero, A., Miften, M., Ten Haken, R. K., Dawson, L. A., Grimm, J., Yorke, E. and Jackson, A. (2021). **Local Control After Stereotactic Body Radiation Therapy for Liver Tumors**. Int J Radiat Oncol Biol Phys *110 (1)*, 188-195, doi: 10.1016/j.ijrobp.2017.12.288.

Padgett, K. R., Simpson, G., Asher, D., Portelance, L., Bossart, E. and Dogan, N. (2020). **Assessment of online adaptive MR-guided stereotactic body radiotherapy of liver cancers**. Phys Med *77*, 54-63, doi: 10.1016/j.ejmp.2020.07.027.

Palacios, M. A., Bohoudi, O., Bruynzeel, A. M. E., van Sorsen de Koste, J. R., Cobussen, P., Slotman, B. J., Lagerwaard, F. J. and Senan, S. (2018). **Role of Daily Plan Adaptation in MR-Guided Stereotactic Ablative Radiation Therapy for Adrenal Metastases**. Int J Radiat Oncol Biol Phys *102 (2)*, 426-433, doi: 10.1016/j.ijrobp.2018.06.002.

Parikh, P. J., Lee, P., Low, D. and Chuong, M. (2018). **Stereotactic MRI-guided On-table Adaptive Radiation Therapy (SMART) for Locally Advanced Pancreatic Cancer**. URL: https://classic.clinicaltrials.gov/show/NCT03621644 [Accessed: 09.02.2024].

Pollard, J. M., Wen, Z., Sadagopan, R., Wang, J. and Ibbott, G. S. (2017). **The future of image-guided radiotherapy will be MR guided**. Br J Radiol *90 (1073)*, 20160667, doi: 10.1259/bjr.20160667.

PR Newswire (2017). ViewRay, Inc. **First Patients Treated with ViewRay's MRIdian Linac System at Henry Ford Health System**. 20.07.2017. URL: https://www.prnewswire.com/news-releases/first-patients-treated-with-viewrays-mridian-linac-system-at-henry-ford-health-system-300491295.html. [Accessed: 20.05.2024].

Raaijmakers, A. J., Raaymakers, B. W. and Lagendijk, J. J. (2005). **Integrating a MRI scanner with a 6 MV radiotherapy accelerator: dose increase at tissue-air interfaces in a lateral magnetic field due to returning electrons**. Phys Med Biol *50 (7)*, 1363-1376, doi: 10.1088/0031-9155/50/7/002.

Raaijmakers, A. J., Raaymakers, B. W. and Lagendijk, J. J. (2008). **Magnetic-field-induced dose effects in MR-guided radiotherapy systems: dependence on the magnetic field strength**. Phys Med Biol *53 (4)*, 909-923, doi: 10.1088/0031-9155/53/4/006.

Raaymakers, B. W., Raaijmakers, A. J., Kotte, A. N., Jette, D. and Lagendijk, J. J. (2004). **Integrating a MRI scanner with a 6 MV radiotherapy accelerator: dose deposition in a transverse magnetic field**. Phys Med Biol *49 (17)*, 4109-4118, doi: 10.1088/0031-9155/49/17/019.

Regnery, S., Buchele, C., Piskorski, L., Weykamp, F., Held, T., Eichkorn, T., Rippke, C., Katharina Renkamp, C., Klüter, S., Ristau, J., König, L., Koerber, S. A., Adeberg, S., Debus, J. and Hörner-Rieber, J. (2022a). **SMART ablation of lymphatic oligometastases in the pelvis and abdomen: Clinical and dosimetry outcomes**. Radiother Oncol *168*, 106-112, doi: 10.1016/j.radonc.2022.01.038.

Regnery, S., Buchele, C., Weykamp, F., Pohl, M., Hoegen, P., Eichkorn, T., Held, T., Ristau, J., Rippke, C., König, L., Thomas, M., Winter, H., Adeberg, S., Debus, J., Klüter, S. and Hörner-Rieber, J. (2021). **Adaptive MR-Guided Stereotactic Radiotherapy is Beneficial for Ablative Treatment of Lung Tumors in High-Risk Locations**. Front Oncol *11*, 757031, doi: 10.3389/fonc.2021.757031.

Regnery, S., Leiner, L., Buchele, C., Hoegen, P., Sandrini, E., Held, T., Deng, M., Eichkorn, T., Rippke, C., Renkamp, C. K., König, L., Lang, K., Adeberg, S., Debus, J., Klüter, S. and Hörner-Rieber, J. (2023). **Comparison of different dose accumulation strategies to estimate organ doses after stereotactic magnetic resonance-guided adaptive radiotherapy**. Radiat Oncol *18 (1)*, 92, doi: 10.1186/s13014-023-02284-7.

Regnery, S., Ristau, J., Weykamp, F., Hoegen, P., Sprengel, S. D., Paul, K. M., Buchele, C., Klüter, S., Rippke, C., Renkamp, C. K., Pohl, M., Meis, J., Welzel, T., Adeberg, S., Koerber, S. A., Debus, J. and Hörner-Rieber, J. (2022b). **Magnetic resonance guided adaptive stereotactic body radiotherapy for lung tumors in ultracentral location: the MAGELLAN trial (ARO 2021-3)**. Radiat Oncol *17 (1)*, 102, doi: 10.1186/s13014-022-02070-x.

Rippke, C., Schrenk, O., Renkamp, C. K., Buchele, C., Hörner-Rieber, J., Debus, J., Alber, M. and Klüter, S. (2022). **Quality assurance for on-table adaptive magnetic resonance guided radiation therapy: A software tool to complement secondary dose calculation and failure modes discovered in clinical routine**. J Appl Clin Med Phys *23 (3)*, e13523, doi: 10.1002/acm2.13523.

Rockoff, S. D. (1977). **The evolving role of computerized tomography in radiation oncology**. Cancer *39 (2 Suppl)*, 694-696, doi: 10.1002/1097-0142(197702)39:2+<694::aid-cncr2820390703>3.0.co;2-6.

Rogowski, P., von Bestenbostel, R., Walter, F., Straub, K., Nierer, L., Kurz, C., Landry, G., Reiner, M., Auernhammer, C. J., Belka, C., Niyazi, M. and Corradini, S. (2021). **Feasibility and Early Clinical Experience of Online Adaptive MR-Guided**

Radiotherapy of Liver Tumors. Cancers (Basel) *13 (7)*, doi: 10.3390/cancers13071523.

Rouffiac Thouant, M. and Rederstorff, E. (2020). **Adaptative MR-Guided Stereotactic Body Radiotherapy of Liver Tumors (RASTAF)**. URL: https://classic.clinicaltrials.gov/show/NCT04242342 [Accessed: 08.02.2024].

Rudra, S., Jiang, N., Rosenberg, S. A., Olsen, J. R., Roach, M. C., Wan, L., Portelance, L., Mellon, E. A., Bruynzeel, A., Lagerwaard, F., Bassetti, M. F., Parikh, P. J. and Lee, P. P. (2019). **Using adaptive magnetic resonance image-guided radiation therapy for treatment of inoperable pancreatic cancer**. Cancer Med *8 (5)*, 2123-2132, doi: 10.1002/cam4.2100.

Rusthoven, K. E., Kavanagh, B. D., Cardenes, H., Stieber, V. W., Burri, S. H., Feigenberg, S. J., Chidel, M. A., Pugh, T. J., Franklin, W., Kane, M., Gaspar, L. E. and Schefter, T. E. (2009). **Multi-institutional phase I/II trial of stereotactic body radiation therapy for liver metastases**. J Clin Oncol *27 (10)*, 1572-1578, doi: 10.1200/JCO.2008.19.6329.

Schneiders, F. L., van Vliet, C., Giraud, N., Bruynzeel, A. M. E., Slotman, B. J., Palacios, M. A. and Senan, S. (2023). **Clinical outcomes of MR-guided adrenal stereotactic ablative radiotherapy with preferential sparing of organs at risk**. Clin Transl Radiat Oncol *43*, 100680, doi: 10.1016/j.ctro.2023.100680.

Solberg, T., Siddon, R. and Kavanagh, B. (2012). **Historical Development of Stereotactic Ablative Radiotherapy**. In, pp. 9-35.

Spindeldreier, C. K., Kluter, S., Hoegen, P., Buchele, C., Rippke, C., Tonndorf-Martini, E., Debus, J. and Horner-Rieber, J. (2021). **MR-guided radiotherapy of moving targets**. Radiologe, doi: 10.1007/s00117-020-00781-4.

Sritharan, K. and Tree, A. (2022). **MR-guided radiotherapy for prostate cancer: state of the art and future perspectives**. Br J Radiol *95 (1131)*, 20210800, doi: 10.1259/bjr.20210800.

Stumpf, P. K., Yorke, E. D., El Naqa, I., Cuneo, K. C., Grimm, J. and Goodman, K. A. (2021). **Modeling of Tumor Control Probability in Stereotactic Body Radiation Therapy for Adrenal Tumors**. Int J Radiat Oncol Biol Phys *110 (1)*, 217-226, doi: 10.1016/j.ijrobp.2020.05.062.

Su, T. S., Liu, Q. H., Zhu, X. F., Liang, P., Liang, S. X., Lai, L., Zhou, Y., Huang, Y., Cheng, T. and Li, L. Q. (2021). **Optimal stereotactic body radiotherapy dosage for hepatocellular carcinoma: a multicenter study**. Radiat Oncol *16 (1)*, 79, doi: 10.1186/s13014-021-01778-6.

Teoh, S., George, B., Owens, R., Bungay, H., Maughan, T. S. and Mukherjee, S. (2022). **Dosimetric Impact of Gastrointestinal Tract Variability during Online Adaptive MR-Guided Hypofractionated Stereotactic Ablative Radiotherapy (SABR) to the Pancreas**. International Journal of Radiation Oncology Biology Physics *114 (3)*, E599-E599, doi: 10.1016/j.ijrobp.2022.07.2293.

Thomas, T. O., Hasan, S., Small, W., Jr., Herman, J. M., Lock, M., Kim, E. Y., Mayr, N. A., Teh, B. S. and Lo, S. S. (2014). **The tolerance of gastrointestinal organs to stereotactic body radiation therapy: what do we know so far?** J Gastrointest Oncol *5 (3)*, 236-246, doi: 10.3978/j.issn.2078-6891.2014.024.

Timmerman, R., McGarry, R., Yiannoutsos, C., Papiez, L., Tudor, K., DeLuca, J., Ewing, M., Abdulrahman, R., DesRosiers, C., Williams, M. and Fletcher, J. (2006). **Excessive toxicity when treating central tumors in a phase II study of stereotactic body radiation therapy for medically inoperable early-stage lung cancer**. J Clin Oncol *24 (30)*, 4833-4839, doi: 10.1200/JCO.2006.07.5937.

Tyagi, N., Liang, J., Burleson, S., Subashi, E., Godoy Scripes, P., Tringale, K. R., Romesser, P. B., Reyngold, M. and Crane, C. H. (2021). **Feasibility of ablative stereotactic body radiation therapy of pancreas cancer patients on a 1.5 Tesla magnetic resonance-linac system using abdominal compression**. Phys Imaging Radiat Oncol *19*, 53-59, doi: 10.1016/j.phro.2021.07.006.

Uchinami, Y., Kanehira, T., Fujita, Y., Miyamoto, N., Yokokawa, K., Koizumi, F., Shido, M., Takahashi, S., Otsuka, M., Yasuda, K., Taguchi, H., Nakazato, K., Kobashi, K., Katoh, N. and Aoyama, H. (2023). **Evaluation of short-term gastrointestinal motion and its impact on dosimetric parameters in stereotactic body radiation therapy for pancreatic cancer**. Clin Transl Radiat Oncol *39*, 100576, doi: 10.1016/j.ctro.2023.100576.

Wang, Y., Mazur, T. R., Green, O., Hu, Y., Li, H., Rodriguez, V., Wooten, H. O., Yang, D., Zhao, T., Mutic, S. and Li, H. H. (2016). **A GPU-accelerated Monte Carlo dose calculation platform and its application toward validating an MRI-guided radiation therapy beam model**. Med Phys *43 (7)*, 4040, doi: 10.1118/1.4953198.

Wen, N., Kim, J., Doemer, A., Glide-Hurst, C., Chetty, I. J., Liu, C., Laugeman, E., Xhaferllari, I., Kumarasiri, A., Victoria, J., Bellon, M., Kalkanis, S., Siddiqui, M. S. and Movsas, B. (2018). **Evaluation of a magnetic resonance guided linear accelerator for stereotactic radiosurgery treatment**. Radiother Oncol *127 (3)*, 460-466, doi: 10.1016/j.radonc.2018.04.034.

Weykamp, F., Hoegen, P., Regnery, S., Katsigiannopulos, E., Renkamp, C. K., Lang, K., König, L., Sandrini, E., Meixner, E., Rippke, C., Buchele, C., Liermann, J., Debus, J., Klüter, S. and Hörner-Rieber, J. (2023). **Long-Term Clinical Results of MR-Guided Stereotactic Body Radiotherapy of Liver Metastases**. Cancers (Basel) *15 (10)*, doi: 10.3390/cancers15102786.

Weykamp, F., Katsigiannopulos, E., Piskorski, L., Regnery, S., Hoegen, P., Ristau, J., Renkamp, C. K., Liermann, J., Forster, T., Lang, K., König, L., Rippke, C., Buchele, C., Debus, J., Klüter, S. and Hörner-Rieber, J. (2022). **Dosimetric Benefit of Adaptive Magnetic Resonance-Guided Stereotactic Body Radiotherapy of Liver Metastases**. Cancers (Basel) *14 (24)*, doi: 10.3390/cancers14246041.

Wittman, D., Paulson, E. S., Eastwood, D., Banerjee, A., Banla, L. I., Schultz, C. J., Awan, M. J., Chen, X., Omari, E., Straza, M. W., Li, A., Erickson, B. A. and Hall, W. A. (2021). **Quantification and Dosimetric Impact of Normal Organ Motion During Adaptive Radiation Therapy Plan Verification Using a 1.5 Tesla Magnetic Resonance Equipped Linear Accelerator (MR LINAC)**. International Journal of Radiation Oncology Biology Physics *111 (3)*, S48-S49, doi: 10.1016/j.ijrobp.2021.07.130.

Zhang, Y., Balter, J., Dow, J., Cao, Y., Lawrence, T. S. and Kashani, R. (2023). **Development of an abdominal dose accumulation tool and assessments of accumulated dose in gastrointestinal organs**. Phys Med Biol *68 (7)*, doi: 10.1088/1361-6560/acbc61.

8 OWN CONTRIBUTION TO DATA COLLECTION AND EVALUATION

Selection of patients, data collection and evaluation were performed by me. MATLAB scripts used for dosimetric and geometric analysis were also written by me. Rouven Behnisch from the Institute of Medical Biometry advised on methods for statistical testing and statistical tests in R were performed by me. The study was designed with help the of Sebastian Klüter and Markus Alber.

9 OWN PUBLICATIONS

Parts of the dosimetric analysis with twenty patients with abdominal lesions directly next to organs at risk and the predictability analysis of organ at risk movement during adaptation will be published in:

Buchele, C., Renkamp, C. K., Regnery, S., Behnisch, R., Rippke, C., Schlüter, F., Hoegen-Saßmannshausen, P., Debus, J., Hörner-Rieber, J., Alber, M. and Klüter, S. (2024). **Intrafraction organ movement in adaptive MR-guided radiotherapy of abdominal lesions – dosimetric impact and how to detect its extent in advance**. Submitted to Radiation Oncology. Revised manuscript currently under review.

It has been submitted to Radiation Oncology and is currently under review. The publication is mainly based on the evaluation of differences in organ at risk dose caused by intrafractional changes presented in chapters 2.1.3 and 3.1.2. Furthermore the analysis of agreement between organ movement during simulation and adaptation as well as correlation between simulation time and magnitude of organ movement as presented in more detail in chapters 2.2 and 3.2 were included in the publication. Some parts of the discussion covering the impact of intrafractional dose changes and the possibility to predict range of movement during adaptation were also included in this publication. This also includes the possible consequences for OAR dose constraints used in MRgRT, the possibility to create PRVs with the method described to determine RoM and possible effects of reduced adaptation times. My contributions to this publication included design of the study, collection, analysis and interpretation of data as well as writing the first draft of the manuscript and revision. The paper will be published under a creative commons attribution 4.0 license, which allows use and adaptation of the paper including images in any format if they are appropriately cited.

A list of further publications is provided below.

Publications

Fink, C. A., Buchele, C., Baumann, L., Liermann, J., Hoegen, P., Ristau, J., Regnery, S., Sandrini, E., König, L., Rippke, C., Bonekamp, D., Schlemmer, H. P., Debus, J., Koerber, S. A., Klüter, S. and Hörner-Rieber, J. (2024). **Dosimetric benefit of online treatment plan adaptation in stereotactic ultrahypofractionated MR-guided radiotherapy for localized prostate cancer**. Front Oncol *14*, 1308406, doi: 10.3389/fonc.2024.1308406.

Hoegen, P., Katsigiannopulos, E., Buchele, C., Regnery, S., Weykamp, F., Sandrini, E., Ristau, J., Liermann, J., Meixner, E., Forster, T., Renkamp, C. K., Schlüter, F., Rippke, C., Debus, J., Klüter, S. and Hörner-Rieber, J. (2023). **Stereotactic magnetic resonance-guided online adaptive radiotherapy of adrenal metastases combines high ablative doses with optimized sparing of organs at risk.** Clin Transl Radiat Oncol 39, 100567, doi: 10.1016/j.ctro.2022.100567.

Klavsen, M. F., Ankjaergaard, C., Boye, K., Behrens, C. P., Vogelius, I. R., Ehrbar, S., Baumgartl, M., Rippke, C., Buchele, C., Renkamp, C. K., Santurio, G. V. and Andersen, C. E. (2023). **Accumulated dose implications from systematic dose-rate transients in gated treatments with Viewray MRIdian accelerators.** Biomed Phys Eng Express 9 (6), doi: 10.1088/2057-1976/acf138.

Regnery, S., Buchele, C., Piskorski, L., Weykamp, F., Held, T., Eichkorn, T., Rippke, C., Katharina Renkamp, C., Klüter, S., Ristau, J., König, L., Koerber, S. A., Adeberg, S., Debus, J. and Hörner-Rieber, J. (2022a). **SMART ablation of lymphatic oligometastases in the pelvis and abdomen: Clinical and dosimetry outcomes.** Radiother Oncol 168, 106-112, doi: 10.1016/j.radonc.2022.01.038.

Regnery, S., Buchele, C., Weykamp, F., Pohl, M., Hoegen, P., Eichkorn, T., Held, T., Ristau, J., Rippke, C., König, L., Thomas, M., Winter, H., Adeberg, S., Debus, J., Klüter, S. and Hörner-Rieber, J. (2021). **Adaptive MR-Guided Stereotactic Radiotherapy is Beneficial for Ablative Treatment of Lung Tumors in High-Risk Locations.** Front Oncol 11, 757031, doi: 10.3389/fonc.2021.757031.

Regnery, S., Katsigiannopulos, E., Hoegen, P., Weykamp, F., Sandrini, E., Held, T., Deng, M., Eichkorn, T., Buchele, C., Rippke, C., Renkamp, C. K., König, L., Lang, K., Thomas, M., Winter, H., Adeberg, S., Klüter, S., Debus, J. and Hörner-Rieber, J. (2023a). To fly or not to fly: **Stereotactic MR-guided adaptive radiotherapy effectively treats ultracentral lung tumors with favorable long-term outcomes.** Lung Cancer 179, 107175, doi: 10.1016/j.lungcan.2023.03.011.

Regnery, S., Leiner, L., Buchele, C., Hoegen, P., Sandrini, E., Held, T., Deng, M., Eichkorn, T., Rippke, C., Renkamp, C. K., König, L., Lang, K., Adeberg, S., Debus, J., Klüter, S. and Hörner-Rieber, J. (2023b). **Comparison of different dose accumulation strategies to estimate organ doses after stereotactic magnetic resonance-guided adaptive radiotherapy.** Radiat Oncol 18 (1), 92, doi: 10.1186/s13014-023-02284-7.

Regnery, S., Ristau, J., Weykamp, F., Hoegen, P., Sprengel, S. D., Paul, K. M., Buchele, C., Klüter, S., Rippke, C., Renkamp, C. K., Pohl, M., Meis, J., Welzel, T., Adeberg, S., Koerber, S. A., Debus, J. and Hörner-Rieber, J. (2022b). **Magnetic resonance guided adaptive stereotactic body radiotherapy for lung tumors in ultracentral location: the MAGELLAN trial (ARO 2021-3).** Radiat Oncol 17 (1), 102, doi: 10.1186/s13014-022-02070-x.

Renkamp, C. K., Eulenstein, D., Sebald, M., Schlüter, F., Buchele, C., Rippke, C., Debus, J. and Klüter, S. (2024). **Evaluation of 2D ion chamber arrays for patient specific quality assurance using a static phantom at a 0.35 T MR-Linac.** Z Med Phys, doi: 10.1016/j.zemedi.2023.12.003.

Rippke, C., Renkamp, C. K., Attieh, C., Schlüter, F., Buchele, C., Debus, J., Alber, M. and Klüter, S. (2023a). **Leaf-individual calibration for a double stack multileaf collimator in photon radiotherapy.** Physics and Imaging in Radiation Oncology 27, doi: 10.1016/j.phro.2023.100477.

Rippke, C., Renkamp, C. K., Stahl-Arnsberger, C., Miltner, A., Buchele, C., Hörner-Rieber, J., Ristau, J., Debus, J., Alber, M. and Klüter, S. (2023b). **A body mass index-based method for "MR-only" abdominal MR-guided adaptive radiotherapy.** Zeitschrift für Medizinische Physik, doi: 10.1016/j.zemedi.2022.12.001.

Rippke, C., Schrenk, O., Renkamp, C. K., Buchele, C., Hörner-Rieber, J., Debus, J., Alber, M. and Klüter, S. (2022). **Quality assurance for on-table adaptive magnetic resonance guided radiation therapy: A software tool to complement secondary dose calculation and failure modes discovered in clinical routine.** J Appl Clin Med Phys 23 (3), e13523, doi: 10.1002/acm2.13523.

Spindeldreier, C. K., Klüter, S., Hoegen, P., Buchele, C., Rippke, C., Tonndorf-Martini, E., Debus, J. and Hörner-Rieber, J. (2021a). **MR-guided radiotherapy of moving targets.** Radiologe, doi: 10.1007/s00117-020-00781-4.

Weykamp, F., Herder-Wagner, C., Regnery, S., Hoegen, P., Renkamp, C. K., Liermann, J., Rippke, C., Koerber, S. A., König, L., Buchele, C., Klüter, S., Debus, J. and Hörner-Rieber, J. (2022a). **Stereotactic body radiotherapy of lymph node metastases under MR-guidance: First clinical results and patient-reported outcomes.** Strahlenther Onkol 198 (1), 56-65, doi: 10.1007/s00066-021-01834-w.

Weykamp, F., Hoegen, P., Regnery, S., Katsigiannopulos, E., Renkamp, C. K., Lang, K., König, L., Sandrini, E., Meixner, E., Rippke, C., Buchele, C., Liermann, J., Debus, J., Klüter, S. and Hörner-Rieber, J. (2023a). **Long-Term Clinical Results of MR-Guided Stereotactic Body Radiotherapy of Liver Metastases.** Cancers (Basel) 15 (10), doi: 10.3390/cancers15102786.

Weykamp, F., Katsigiannopulos, E., Piskorski, L., Regnery, S., Hoegen, P., Ristau, J., Renkamp, C. K., Liermann, J., Forster, T., Lang, K., König, L., Rippke, C., Buchele, C., Debus, J., Klüter, S. and Hörner-Rieber, J. (2022b). **Dosimetric Benefit of Adaptive Magnetic Resonance-Guided Stereotactic Body Radiotherapy of Liver Metastases.** Cancers (Basel) 14 (24), doi: 10.3390/cancers14246041.

10 ACKNOWLEDGEMENT

This is where I would like to thank everyone who has supported me over the last few years and allowed me to complete this thesis.

In particular, I would like to thank Prof. Dr. Markus Alber and Dr. Sebastian Klüter for their guidance and the numerous discussions that have been a great help to me.

Additionally, I am grateful to Prof. Dr. Juliane Hörner-Rieber for her support with medical as well as any other question I had during the course of this work.

I would also like to thank the MR-linac team, Dr. Katharina Renkamp, Dr. Carolin Rippke and Fabian Schlüter, who enabled me to concentrate fully on my thesis, especially towards the end. Without you, the last few years would have been much less enjoyable.

And finally, I am grateful to my family who have supported me through all the ups and downs of the last few years. They were always there for me, especially when I got stuck on some issue or another.

EIDESSTATTLICHE VERSICHERUNG

1. Bei der eingereichten Dissertation zu dem Thema

“Daily adaptive magnetic resonance guided radiotherapy – analysis of patient benefit”

handelt es sich um meine eigenständig erbrachte Leistung.

2. Ich habe nur die angegebenen Quellen und Hilfsmittel benutzt und mich keiner unzulässigen Hilfe Dritter bedient. Insbesondere habe ich wörtlich oder sinngemäß aus anderen Werken übernommene Inhalte als solche kenntlich gemacht.

3. Die Arbeit oder Teile davon habe ich bislang nicht an einer Hochschule des In- oder Auslands als Bestandteil einer Prüfungs- oder Qualifikationsleistung vorgelegt.

4. Die Richtigkeit der vorstehenden Erklärungen bestätige ich.

5. Die Bedeutung der eidesstattlichen Versicherung und die strafrechtlichen Folgen einer unrichtigen oder unvollständigen eidesstattlichen Versicherung sind mir bekannt. Ich versichere an Eides statt, dass ich nach bestem Wissen die reine Wahrheit erklärt und nichts verschwiegen habe.

Ort und Datum Unterschrift